Topological superconducting phases in one dimension

Felix von Oppen, Yang Peng, Falko Pientka

Dahlem Center for Complex Quantum Systems and Fachbereich Physik, Freie Universität Berlin, Arnimallee 14, 14195 Berlin, Germany

OXFORD
UNIVERSITY PRESS

Contents

1
Introduction

These lecture notes attempt to give a pedagogical account of the basic physics of Majorana bound states and the topological superconductors which host them. They introduce the basic concepts as well as possible experimental realizations, emphasizing one-dimensional systems which much of the current experimental activity is focused on. In writing these notes, we preferred simple arguments and explicit derivations that illustrate the main points rather than the theoretically most pleasing or general approach. The notes are emphatically not a review, and referencing is not meant to be complete or to accurately reflect the development of the field. Much more complete lists of references can be found in the original literature [1–4].

1.1 Motivation

Bosons are frequently their own antiparticles. Quite distinctly, no elementary fermion is known to have this property. A long time ago, Majorana developed a theoretical description of fermions which are their own antiparticles [5]. Ever since, there have been attempts to find such particles in nature, with neutrinos being the most likely candidate [6]. These experiments typically search for neutrinoless double-β decays (Fig. 1.1). In a β-decay, a neutron decays into a proton, an electron, and a neutrino. In a neutrinoless double-β decay, two neutrons would be decaying into two protons and two electrons without emitting any neutrinos. A neutrinoless double-β decay is only possible when the neutrino is its own antiparticle and hence a Majorana fermion. Indeed, when a particle is its own antiparticle, creating and annihilating this particle is in some sense the same process. Then, the neutrino virtually emitted by one neutron can be absorbed in the β-decay of the other neutron, with no real neutrino created in the process. To date, no experiment could convincingly detect such a neutrinoless double-β decay.

In these notes, we are concerned with Majorana bound states. Unlike the particles that Majorana envisioned, these do not have any dynamics of their own in that they do not possess a dispersion as a function of a momentum quantum number. But they do share the property that annihilating and creating these excitations is described by the same operator,

$$\gamma = \gamma^\dagger, \tag{1.1}$$

i.e., γ is a hermitian operator. As these bound states do not have any dynamics of their own, we can simply label them as γ_j with $j = 1, 2, 3, \ldots$, where j enumerates, say, their locations. In a way, these condensed matter Majoranas are even more exotic and interesting than their high-energy counterparts. This is because of two of their

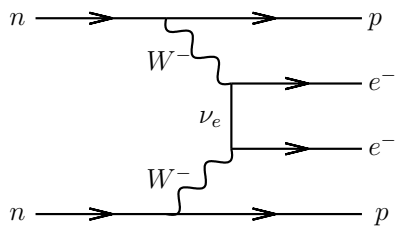

Fig. 1.1 Double-β decay is only possible when neutrinos are their own antiparticles. Then, the two neutrinos which are virtually emitted by the two neutrons can mutually annihilate.

essential properties: First, spatially isolated Majorana bound states have zero excitation energy with non-Majorana excitations separated by a finite energy gap. Thus, the existence of isolated Majorana bound states necessarily implies that the many-body ground state of the system is multiply degenerate. These degeneracies are highly nonlocal in that each twofold degeneracy of the ground state is associated with the existence of *two* Majorana bound states. Second, their quantum statistics turns out to be neither bosonic nor fermionic but rather of a new type called nonabelian quantum statistics. When exchanging (also termed braiding) two Majorana bound states, the many-body state of the system neither remains unchanged (as for bosons) nor is it multiplied by a minus sign (as for fermions) nor even multiplied by a general phase factor (as for abelian anyons). Instead, it undergoes a unitary rotation in the degenerate ground-state subspace. As is typical for rotations in higher dimensions, these unitary transformations within the ground-state manifold generally do not commute, hence the name nonabelian statistics.

It is these two properties that make Majoranas attractive building blocks for topological quantum information processing [7,8]. In his seminal work [7], Kitaev envisioned to encode the quantum information within the degenerate ground state manifold associated with the Majoranas and to process this information by means of braiding operations. Recall that the ground-state degeneracy associated with the Majoranas is robust as long as the Majoranas remain spatially isolated. This implies in particular that this degeneracy remains unaffected by local perturbations of the system, such as electric or magnetic fields and that there are no relative dynamical phases which spoil the phase relations between different components of the many-body wavefunction within the ground-state manifold – at least as long as the fields vary adiabatically in time on the scale of the gap. This robustness to perturbing electric and magnetic fields can be thought of intuitively as a consequence of the Majoranas being their own antiparticles. Such particles can carry neither charge nor spin, as both would reverse sign for the antiparticle, and are thus unaffected by external fields.

The insensitivity to fields leads to a high degree of (topological) protection of the encoded quantum transformation against decoherence. But it also means that these fields cannot be used to manipulate this information. Instead, one hopes to use braiding operations of the Majorana bound states to manipulate the quantum information. Due to their nonabelian statistics, such braiding operations effect unitary operations within the degenerate ground-state manifold and thus manipulation of the encoded

quantum information. Just as the information storage is topologically protected, so is this strategy of information processing. Indeed, the effect of the braiding operation is insensitive to the specific geometry of the exchange path but depends only on its topology, i.e., the fact that we exchange two of the Majoranas.

Let us briefly address two concerns that one might have about this scheme. The first is simple: How does one braid the Majoranas given that they are insensitive to magnetic and electric fields? While the energy of the Majorana bound state is indeed insensitive to electric and magnetic fields, the position of the bound state is not! This is because the bound state is usually localized near a defect of the underlying phase, such as a domain wall or a superconducting vortex, and these defects can be moved by the application of electric or magnetic fields. The second concern turns out to be more serious: For a quantum computer to be universal, braiding operations must be able to implement any possible unitary transformation within the ground-state manifold. This is actually not the case for Majorana bound states. Thus, building a universal quantum computer based on Majoranas requires one to perform some operations in ways which are not topologically protected. Nevertheless, it turns out that one may still gain significantly from performing only a subset of operations in a topologically protected manner.

Above, we introduced the creation and annihilation operators associated with Majorana bound states through Eq. (1.1). In fact, any ordinary fermionic system can be discussed in terms of such operators. To see this, just note that we can always decompose conventional fermionic operators c_j (satisfying the anticommutation relations $\{c_i, c_j\} = \{c_i^\dagger, c_j^\dagger\} = 0$ and $\{c_i, c_j^\dagger\} = \delta_{ij}$) into their hermitian and antihermitian parts,

$$c_j = \frac{1}{2}(\gamma_{2j-1} + i\gamma_{2j}), \tag{1.2}$$

just as complex numbers can be decomposed into their real and imaginary parts. (The factor of $1/2$ is a convention.) Here, all γ_j are hermitian operators, satisfying $\gamma_j = \gamma_j^\dagger$, and we have written the antihermitian part of c_j as $i\gamma_{2j}$. Expressing the γ_j in terms of the original fermion operators by inverting Eq. (1.2), one readily finds that the γ_j satisfy the Majorana anticommutation relations

$$\{\gamma_i, \gamma_j\} = 2\delta_{ij}. \tag{1.3}$$

If we can discuss any fermionic system in terms of Majorana operators, what is so special about them? The answer is twofold: First, we will be concerned with situations, in which the Majorana operators are eigenoperators of the system. In a generic fermionic system, the Majorana operators introduced through Eq. (1.2) are not eigenoperators. Second, the Majoranas introduced in this fashion do not correspond to spatially isolated bound states of the system. In contrast, the spatial isolation is absolutely essential for all the special properties of the Majorana bound states which we discuss in these notes.

The Majorana anticommutation relation can be used to amplify the difference between Majoranas on the one side and fermions and bosons on the other. Eq. (1.3) implies that $(\gamma_j^\dagger)^2 = 1$. Thus, creating two Majoranas of the same kind brings the system back to the state it started from. This is of course eminently reasonable for

a particle which is its own antiparticle – the second Majorana simply annihilates the first. On the other hand, this is very different from bosons or fermions. Fermions satisfy the Pauli principle which implies that conventional fermionic operators square to zero. Adding two bosons to some (Fock) state by multiplying it by the square of a boson creation operator takes the system into a state which is orthogonal to the original one.

There have recently been numerous experiments which provided possible evidence for Majorana bound states [9–17]. Many of these experiments are based on one-dimensional electron systems coupled to conventional s-wave superconductors. These notes focus on this class of systems. While there is substantial reason to be optimistic, the interpretation of many of these experiments is currently still under debate. For this reason, we will refrain from a detailed discussion of these experiments. Instead, we aim at providing the background knowledge required for understanding the experimental systems and the Majorana signatures that they are based on, allowing the reader of these notes to come up with their own judgment.

These lecture notes are organized as follows. The remainder of the Introduction will be concerned with heuristic considerations where one might reasonably look for Majorana bound states. Section 2 is concerned with simple model systems which exhibit Majorana bound states. We will focus on one-dimensional systems where Majoranas are associated with domain walls between topological and nontopological superconducting phases. While these models seem rather removed from experiment at first, it is now clear that they can be effectively realized in experimentally relevant systems. This is discussed at length in Secs. 3, 4, and 5, which are concerned with proximity-coupled topological-insulator edges, semiconductor quantum wires, and chains of magnetic adatoms, respectively . Section 6 discusses how to manipulate Majorana bound states and derives their nonabelian statistics explicitly in a particularly simple setting. Section 7 discusses some popular techniques how to detect Majorana bound states in experiment. We conclude in Sec. 8.

1.2 Heuristic arguments

Let us start with a heuristic argument where we might be looking for Majorana excitations which are their own antiparticle, i.e., whose creation and annihilation operators satisfy $\gamma = \gamma^\dagger$. The building blocks at our disposal in a conventional metal or semiconductor material are electrons and holes which can be viewed as particles and antiparticles. An excitation which is its own antiparticle should therefore consist in equal parts of electrons and holes. One such excitation in the solid state is the exciton, a bound state of an electron in the conduction band and a hole in the valence band. However, excitons are bound states of two fermions. These are created by products of two fermionic operators, and can thus be approximately described as bosonic excitations.

In order to realize Majorana excitations, we therefore need to consider operators satisfying $\gamma = \gamma^\dagger$ which are linear in the original fermionic operators. Such an operator which consists in equal parts of electrons and holes is[1]

[1] This is obviously not unique. We could also consider operators such as $i(c - c^\dagger)$ or $e^{i\varphi}c + e^{-i\varphi}c^\dagger$. This is not essential for the heuristic argument in this section.

$$\gamma = c + c^\dagger. \tag{1.4}$$

Written in this form, it becomes clear that we should be looking for Majorana excitations in BCS superconductors. As is familiar from the BCS theory of superconductivity, these have fermionic quasiparticle excitations described by linear combinations of creation and annihilation operators,

$$\gamma = uc + vc^\dagger. \tag{1.5}$$

The prefactors in this linear combination depend on the energy of the (Bogoliubov) quasiparticle excitation.

An excitation far above the superconducting gap will be only weakly affected by the superconducting correlations and consequently behave, to a good approximation, like an electron. We expect that annihilating such an excitation is essentially equivalent to annihilating an electron, and thus $u \approx 1$ and $v \approx 0$. Similarly, an excitation in the Fermi sea far below the superconducting gap will essentially look like a hole. To a good approximation, annihilating such an excitation just corresponds to filling the hole, i.e., we have $u \approx 0$ and $v \approx 1$. A Majorana excitation has equal amplitudes of c and $c^\dagger$, i.e., we are looking for an excitation with $u = v$.[2] In view of the energy dependence of the prefactors u and v, it is natural to expect $u = v$ halfway in between the electron-like and the hole-like excitations, i.e., for midgap excitations with excitation energy $E = 0$. We should thus be looking for Majoranas as zero-energy excitations in superconductors.

An attentive reader might object that these arguments do not make sense. The argument neglects the fact that electrons have spin and so do the Bogoliubov quasiparticles. In standard BCS theory, the Bogoliubov quasiparticles have the form

$$\gamma_\uparrow = uc_\uparrow + vc_\downarrow^\dagger, \tag{1.6}$$

which differs from Eq. (1.5) by the spin labels. Clearly, the spin indices spoil the Majorana property, i.e., these spinful Bogoliubov operators are no longer equal to their adjoint, $\gamma_\uparrow \neq \gamma_\uparrow^\dagger$, even when $u = v$.

However, there is an emergency exit that allows us to save the argument. We simply assume that we are considering BCS pairing of spinless fermions. Then the fermionic operators c and $c^\dagger$ do not have spin indices and Eq. (1.5) is the appropriate operator for the Bogoliubov excitations. Thus, we should be looking for Majoranas as zero-energy excitations in superconductors made of spinless fermions.

Finally, the assumption of spinless fermions immediately has one more consequence. In superconductors, the fermions pair into Cooper pairs. Because of the Pauli principle, the Cooper pair wavefunction must be antisymmetric. In conventional (s-wave) superconductors, this is satisfied because the electrons are in an antisymmetric spin singlet configuration while their orbital wavefunction is a symmetric s-state. For spinless fermions, there is no spin part of the Cooper pair wavefunction and the antisymmetry must be in the orbital part. Then, the pairing symmetry can no longer be s-wave and the simplest antisymmetric option is p-wave pairing.

[2] Or in view of the previous footnote, more accurately $u = v^*$.

Thus, we can finally state where we should be looking for Majoranas: as *zero-energy excitations in spinless p-wave superconductors*!

2
Spinless p-wave superconductors

2.1 Continuum model and phase diagram

Of course, the heuristic arguments of the previous section do not imply that spinless p-wave superconductors host Majoranas. To confirm that this can indeed be the case, we will now study a one-dimensional model of a spinless p-wave superconductors. To be specific, we will look at a continuum mean-field model with many-particle Hamiltonian[1]

$$\mathcal{H} = \int dx \left\{ \psi^\dagger(x) \left(\frac{p^2}{2m} - \mu \right) \psi(x) + \Delta' [\psi^\dagger(x) \partial_x \psi^\dagger(x) + \text{h.c.}] \right\}. \tag{2.1}$$

Here, $\psi^\dagger(x)$ creates a spinless fermion at position x and $\xi_p = p^2/2m - \mu$ is their normal-state dispersion. The pairing of strength Δ' (assumed real for definiteness) is of p-wave nature, as reflected in the presence of the derivative ∂_x in the pairing terms. Note that Δ' has units of velocity. The BdG Hamiltonian associated with the many-body Hamiltonian is (cp. App. A)

$$H = \begin{pmatrix} \xi_p & -i\Delta' p \\ i\Delta' p & -\xi_p \end{pmatrix} = \xi_p \tau_z + \Delta' p \tau_y, \tag{2.2}$$

where $\boldsymbol{\tau}$ denotes the vector of Pauli matrices τ_i in particle-hole space.

We can straightforwardly derive the excitation spectrum of the model from the BdG Hamiltonian. For an infinite system (or a system with periodic boundary conditions), momentum is a good quantum number and we obtain

$$E_k = \pm [\xi_k^2 + \Delta'^2 k^2]^{1/2} \tag{2.3}$$

by diagonalizing the 2×2 BdG Hamiltonian. This spectrum is gapped almost everywhere, except when $\xi_k = 0$ for $k = 0$, i.e., when $\mu = 0$.[2] Of course, the model also becomes gapless in the absence of pairing and any positive chemical potential, i.e., for $\Delta' = 0$ and $\mu > 0$.

[1] Often, one first discusses a lattice version of this model, the so-called Kitaev chain [18]. This is briefly discussed later in these notes in Sec. 5.3. This section can also be read at this point.

[2] Note that this is distinctly different from s-wave pairing for which the excitation spectrum $E_k = \pm[\xi_k^2 + \Delta^2]^{1/2}$ is always gapped for nonzero pairing, regardless of the chemical potential.

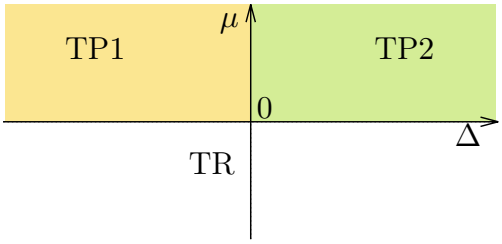

Fig. 2.1 The phase diagram of a one-dimensional p-wave superconductor as function of p-wave pairing strength Δ' and chemical potential μ. There are topological superconducting phases for $\mu > 0$, while the system is topologically trivial for $\mu < 0$. The topological phases at positive μ differ in their winding numbers depending on the sign of Δ'.

The lines $\mu = 0$ as well as $\Delta' = 0$ for $\mu > 0$ delineate topological quantum phase transitions. To make this explicit, rewrite the 2×2 BdG Hamiltonian in Eq. (5.52) as a spin Hamiltonian,

$$H_k = \mathbf{b}_k \cdot \boldsymbol{\tau}, \tag{2.4}$$

where $\mathbf{b}_k$ can be viewed as an effective Zeeman field acting in particle-hole space. According to the BdG-Hamiltonian (5.52), we have

$$(b_k)_x = 0 \ ; \ (b_k)_y = \Delta' k \ ; \ (b_k)_z = \xi_k. \tag{2.5}$$

We can now consider the mapping from reciprocal space $k \in \mathbf{R}$ to the unit vector $\hat{\mathbf{b}}_k = \mathbf{b}_k/|\mathbf{b}_k|$. As the vector $\mathbf{b}_k$ lies in the yz plane and the corresponding unit vector on a circle, there is a topological winding number associated with this mapping, which counts the number of times the image winds around this circle. This mapping is illustrated in Fig. 2.2.

Consider first the case of $\mu < 0$. Then, we have $\xi_k > 0$ for all k and the unit vector $\hat{\mathbf{b}}_k$ remains on the upper half circle for all $k \in \mathbf{R}$, pointing in the positive z-direction for $k = \pm\infty$. Thus, for $\mu < 0$, the unit vector has winding number zero.

Now consider $\mu > 0$. In this case, ξ_k changes sign from positive values at large $|k|$ to negative values near $k = 0$. Similarly, b_y changes sign as k changes from negative to positive. As a result, the unit vector $\hat{\mathbf{b}}_k$ winds once around as k varies from $-\infty$ to $+\infty$. It is also evident that the direction of winding depends on the sign of Δ'. As a result, we have a winding number ± 1 depending on the sign of Δ'.

Thus, we find that the system has one phase – referred to as nontopological or trivial phase – with zero winding number and a topological phase (or more accurately topological phases – see below) with a nonzero winding number. The trivial phase occurs when the chemical potential is below the bottom of the normal-state band. We can change parameters in (a.k.a. deform) the Hamiltonian to the vacuum limit $\mu \to -\infty$ without ever closing the gap. This is a characteristic feature of a trivial gapped phase. In contrast, the topological phase occurs for $\mu > 0$ and there is always a gap closing when deforming the Hamiltonian from the topological phase towards the vacuum limit.

The excitation spectrum also becomes gapless for $\Delta' = 0$. This allows the winding number to change sign along the line $\Delta' = 0$ and $\mu > 0$. Thus, there are two distinct topological phases with opposite signs of the winding number. In fact, more generally, the winding number can take on any value in $\mathbf{Z}$, as long as the Hamiltonian satisfies a chiral symmetry. In the present case, this chiral symmetry is reflected in the fact that the Hamiltonian (2.4) involves only two of the three Pauli matrices, so that

$$\{\tau_x, H_k\} = 0, \tag{2.6}$$

which places this Hamiltonian into symmetry class BDI.[3] Clearly, it is this absence of the third Pauli matrix that makes the unit vector $\hat{\mathbf{b}}_k$ lie in a plane which in turn allows the definition of a winding number.

We could also consider more general Hamiltonians which involve all three Pauli matrices, which fall into symmetry class D. Even in this case, we can define a topological index, which is now a $\mathbf{Z}_2$ index taking on only two distinct values corresponding to the trivial and topological phases. To understand this, it is perhaps easier to consider a lattice system with Brillouin zone $k \in [-\pi/a, \pi/a]$. The essential observation is that in a spinless system, there can be no pairing of the $k = 0$ and $k = \pm\pi/a$ states. The reason is that pairing is between states with opposite momenta. For $k = 0$, the opposite-momentum state would be the state itself. For $k = \pi/a$, this is actually also the case since it differs from its opposite-momentum partner $k = -\pi/a$ by a reciprocal lattice vector, so that the two need to be identified. The absence of pairing at $k = 0$ and $k = \pm\pi/a$ implies that the unit vector $\hat{\mathbf{b}}_k$ necessarily points along the z-direction at these points of the Brillouin zone, either in the positive or the negative z-direction.

Now the mapping from the Brillouin zone to the unit vector $\hat{\mathbf{b}}_k$ is a mapping into the surface of a sphere and there can be two topologically distinct bandstructures, see Fig. 2.3: Either, $\hat{\mathbf{b}}_k$ has the same sign at $k = 0$ and $k = \pm\pi/a$, which corresponds to the trivial phase, or it has opposite signs which happens in the topological phase. Physically, this index measures whether the chemical potential falls within the band or not. Indeed, $k = 0$ and $k = \pm\pi/a$ correspond to minimum and maximum of the normal-state band and the sign of the z-component of $\hat{\mathbf{b}}_k$ is determined by whether the normal-state energy ϵ_k is below or above the chemical potential.

[3] We will not discuss the symmetry classification of topological phases in any detail. The interested reader is referred to the literature [20].

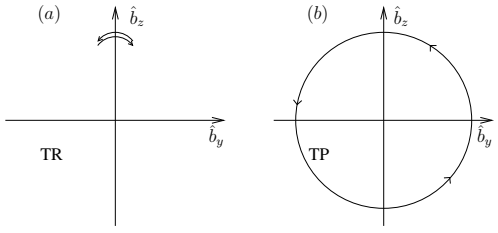

Fig. 2.2 Illustration of the mapping $k \to \hat{\mathbf{b}}_k$ in symmetry class BDI. (a) Trivial or nontopological phase. (b) Topological phase.

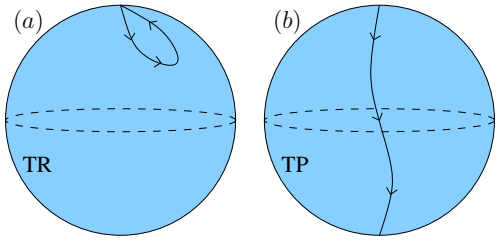

Fig. 2.3 Illustration of the mapping $k \to \hat{\mathbf{b}}_k$ in symmetry class D. (a) Trivial or nontopological phase. (b) Topological phase.

2.2 Domain walls and Majorana excitations

We can induce a domain wall between the topological and the trivial phase by a spatially varying chemical potential. At the domain wall, the chemical potential changes from negative to positive values. Let's assume that μ changes linearly in x in the vicinity of the domain wall,[4]

$$\mu(x) = \alpha x. \tag{2.7}$$

Clearly, the gap in the excitation spectrum vanishes right at the domain wall and increases linearly away from it. Thus, it is natural to suspect that there are bound states trapped at the domain wall.

Quite generally, domain walls between topologically distinct phases are associated with gapless excitations. Examples are the chiral edge states of quantum Hall states or the helical edge states of topological insulators. We will now see explicitly that in the present case, the domain wall is also associated with a gapless excitation and that this gapless excitation is a zero-energy Majorana bound state.

While this is a general property of domain walls in this model, we will only consider a limit in which the calculation becomes particularly simple. Indeed, for a sufficiently smooth domain wall, the relevant momenta in the vicinity of the domain wall are small and we can neglect $p^2/2m$ in the BdG Hamiltonian (2.2).[5] Then, the BdG Hamiltonian of the domain wall takes on the form

$$H = -\alpha x \tau_z + \Delta' p \tau_y. \tag{2.8}$$

This has the form of a Dirac Hamiltonian with a spatially varying mass. In fact, the mass changes sign at the position of the domain wall. Following the seminal work of Jackiw and Rebbi [19] in the context of high-energy physics, this implies under rather general conditions that there is a zero-energy bound state localized at the domain wall.

Indeed, the spectrum of this Dirac Hamiltonian is readily obtained by squaring the Hamiltonian. As any Bogoliubov-deGennes Hamiltonian, the spectrum of H is

[4] It is also straightforward to study domain walls at which the chemical potential jumps abruptly from negative to positive values. It is left as an exercise for the reader to derive the subgap spectrum in this case.

[5] To see this, compare the chemical potential and the pairing term. This implies that there is a characteristic length $\sqrt{\Delta'/\alpha}$ and thus a characteristic energy $\sqrt{\Delta'\alpha}$. Then, the quadratic term is of order $\alpha/m\Delta'$, which is small compared to the characteristic energy as long as $\alpha \ll m^2\Delta'^3$.

symmetric about zero energy, i.e., for any eigenstate with energy E, there is another eigenstate with energy $-E$ (see App. A). Thus, we do not lose any information on the spectrum when squaring the Hamiltonian. Using that the Pauli matrices square to unity and anticommute,

$$\{\tau_i, \tau_j\} = 2\delta_{ij}, \tag{2.9}$$

we obtain

$$H^2 = (\alpha x)^2 + (\Delta' p)^2 - \Delta' \alpha [x, p] \tau_z \tau_y. \tag{2.10}$$

With the commutator $[x, p] = i$ and $\tau_z \tau_y = -i\tau_x$, this simplifies to

$$H^2 = (\alpha x)^2 + (\Delta' p)^2 - \Delta' \alpha \tau_x. \tag{2.11}$$

In the eigenbasis of τ_x (labeled by $\pm$), this is a harmonic-oscillator Hamiltonian up to a shift in energy, and the bound-state spectrum associated with the domain wall becomes

$$(E_n^{\pm})^2 = 2\Delta' \alpha \left(n + \frac{1}{2} \right) \mp \Delta' \alpha. \tag{2.12}$$

In line with general expectations for domain walls between topologically distinct phases, there is an eigenstate with exactly zero energy, $E_0^+ = 0$.

To better understand the quasiparticle excitation which is described by this zero-energy state, let us consider the associated Bogoliubov operator. The zero-energy eigenspinor of the BdG Hamiltonian is

$$\langle x | n = 0, + \rangle = u_0(x) \begin{pmatrix} 1 \\ 1 \end{pmatrix}, \tag{2.13}$$

where $u_0(x)$ is the Gaussian ground-state eigenfunction of the harmonic oscillator, centered at the domain wall. Then, the Bogoliubov operator follows in the usual way, cf. App. A, by "dotting" the bra $\langle n = 0, + |$ into the Nambu spinor, $[\psi(x), \psi^\dagger(x)]^T$. This gives

$$\gamma = \int dx u_0(x) [\psi(x) + \psi^\dagger(x)]. \tag{2.14}$$

This quasiparticle operator does indeed obey the Majorana property $\gamma = \gamma^\dagger$.[6]

2.3 Topological protection and many-body ground state

We have derived the zero-energy Majorana mode only for a special limit in which the calculation becomes particularly simple. It is thus natural to ask how general the result is. As mentioned above, such a zero-energy Majorana state is generically found at any domain wall between the topological and the trivial phase. A simple argument which shows that this must be the case is the following. Consider a semiinfinite 'wire' in the topological phase. The end of the system is a domain wall between the topological phase and the trivial phase as represented by the "vacuum" outside the system. Thus, there is one zero-energy Majorana bound state localized at the end of the wire. Its BdG

[6] Note that we can take the ground-state wavefunction $u_0(x)$ of the harmonic oscillator to be real.

spectrum consists of the zero-energy Majorana state and the symmetric quasiparticle continua outside the gap at positive and negative energies. Imagine that we are now deforming the Hamiltonian by changing its parameters. As long as the gap does not close, the symmetry of the BdG spectrum between positive and negative energies implies that the zero-energy state must stay put at zero energy!

Next consider a system of finite length. Then there are two Majorana bound states, one at each end of the wire. As long as we can neglect the overlap between these two localized Majorana bound states, both Majorana bound states have exactly zero energy. Overlap between the Majorana end states introduces a coupling between them and the two Majorana zero modes can split into two states whose energies are nonzero and symmetric about zero energy. As the Majoranas are exponentially localized, the energy splitting decreases exponentially with the length of the wire.

Now consider a wire which is sufficiently long so that we can neglect the overlap between the Majoranas at its ends. Then, the excitation spectrum has two zero-energy Majorana bound states with their corresponding quasiparticle operators, say, γ_1 and γ_2. We can combine these two Majorana operators into one conventional fermion operator,

$$c = \frac{1}{2}(\gamma_1 + i\gamma_2). \tag{2.15}$$

As usual, this conventional fermion can be either empty or occupied. Since the Majorana bound states have zero excitation energy, both states have exactly the same many-body energy, and we find that there are two degenerate ground states.

Interestingly, these two states differ by fermion number parity. The mean-field Hamiltonian of superconductors break particle-number conservation. Fermion number parity, however, remains a good quantum number, since the pairing terms add or remove particles only in pairs. In conventional superconductors, we expect the ground state to have even fermion parity. Any state with an odd number of fermions would necessarily have one unpaired electron which is less favorable than a fully paired state. In contrast, the two ground states of our wire in a topologically nontrivial superconducting phase differ by the occupation of a single fermion state, so that we have one ground state with even and one ground state with odd fermion number parity. The fermion parity operator can be written as $P = 2c^\dagger c - 1$ with eigenvalues ± 1, or as

$$P = i\gamma_1\gamma_2 \tag{2.16}$$

when written in terms of the Majorana operators.

When there are $2N$ Majorana bound states, we can use the same strategy and group them into N pairs. Each pair of Majorana fermion operators γ_{2j-1} and γ_{2j} can be combined into a conventional fermion operator c_j. Each of these conventional fermion states can now be empty or occupied, leading to an overall ground state degeneracy of 2^N. These states can again be grouped according to fermion parity. The fermion parity operator is just the product over the fermion parity operators $2c_j^\dagger c_j - 1$ for each pair so that

$$P = i^N \gamma_1 \gamma_2 \ldots \gamma_{2N}. \tag{2.17}$$

Thus, there are 2^{N-1} ground states of either parity.

2.4 Experimentally accessible systems

While it is perhaps theoretically pleasing that spinless p-wave superconductors host Majorana excitations, this result may seem rather unphysical. First and foremost, electrons do have spin. Second, the vast majority of superconductors in nature are s-wave, and there are only very few p-wave superconductors. Moreover, we will be looking for Majoranas in one-dimensional systems for which strictly speaking, the mean-field BCS theory underlying these arguments is not appropriate due to strong order-parameter fluctuations.

Nevertheless, starting with the seminal work of Fu and Kane [21,22], it has become abundantly clear that this scenario can be realized experimentally in a variety of systems. The basic physical ingredients are the same in all of these platforms:

- proximity coupling to a conventional s-wave superconductor
- spin polarization
- spin-orbit coupling

Employing proximity-induced superconductivity makes it appropriate to discuss the one-dimensional systems within mean-field theory as the superconducting correlations are inherited from a bulk superconductor. Spin-polarized electron systems are a close relative to spinless fermion systems. Of course, there is a conflict in that it is impossible to proximity-induce s-wave pairing in a spin-polarized system. The reason is that in order to satisfy the Pauli principle, the Cooper pairs are spin singlets. Such spin-singlet Cooper pairs obviously cannot enter into a spin-polarized system by spin-conserving processes.

This conflict is really an opportunity when involving spin-orbit coupling. To understand this, it might be simplest to locate the spin-orbit coupling in the superconductor rather than the one-dimensional system. Then, orbital angular momentum is no longer a good quantum number in the superconductor and there can be a small p-wave admixture to the s-wave pairing. Unlike the s-wave correlations, the p-wave correlations can transfer to the spin-polarized system. As a result, the one-dimensional system effectively develops p-wave superconducting correlations by proximity.

In fact, the conditions for realizing topological superconductivity are less stringent than this argument may make it appear. For instance, the spin-orbit coupling can be in the proximitizing superconductor or in the one-dimensional system, and the assumption of full spin polarization can be relaxed. In the three following chapters, we will discuss some of the platforms which are most actively pursued in experiment.

3
Topological insulator edges

3.1 Model and phases

We start illustrating the physics outlined at the end of the last section by 2d topological insulators, proximity coupled to an s-wave superconductor [22]. We assume that the Fermi energy is in the gap of the topological insulator so that the only relevant electronic degrees of freedom are the helical edge states. Thus, there is just a single spin channel propagating in each direction at the Fermi energy, and there is perfect spin-orbit coupling as the propagation direction is directly tied to the spin polarization. We can gap out these edge states in two different ways, namely by proximity coupling to an s-wave superconductor and by applying a Zeeman field in a direction perpendicular to the spin quantization direction of the edge states.

The corresponding BdG Hamiltonian of the proximity-coupled topological insulator edge takes the form (see App. A)

$$H = v_F p \sigma_x \tau_z - B\sigma_z + \Delta\tau_x. \tag{3.1}$$

Here, σ_i denotes Pauli matrices in spin space. We assume that the helical edge states are polarized along the x-direction, while the Zeeman field is applied in the z-direction. The τ_i still denote Pauli matrices in particle-hole (Nambu) space. This way of writing the Hamiltonian assumes that we write the Nambu spinors as $[\psi_\uparrow, \psi_\downarrow, \psi_\downarrow^\dagger, -\psi_\uparrow^\dagger]^T$, see App. A. For simplicity, we choose the chemical potential to be at $\mu = 0$ and thus right at the Dirac point associated with the edge states.

In the Hamiltonian (3.1), we have accounted for the proximity coupling to the superconductor through the induced s-wave gap Δ. In a more microscopic theory, we would describe both the topological insulator and the superconductor, including the coupling between the two. It turns out that with certain caveats, this can then be reduced to the form of Eq. (3.1). For the most part, we will introduce the proximity-induced pairing correlations in the simplified manner of Eq. (3.1). The more microscopic approach is sketched in App. B. We also need to rely on the microscopic approach in Sec. 5 when discussing chains of magnetic adatoms.

We can again obtain the spectrum of Hamiltonian (3.1) by squaring it. This yields

$$H^2 = (v_F p)^2 + B^2 + \Delta^2 - 2B\Delta\sigma_z\tau_x \tag{3.2}$$

and thus

$$E_k = \pm\sqrt{(v_F k)^2 + (\Delta \pm B)^2}, \tag{3.3}$$

where all combinations of signs are possible. Note that the gap closes for $B = \pm\Delta$, showing that the gaps due to Δ and B compete. This gap closing signals a topological phase transition.

At first sight, it may appear that the Hamiltonian (3.1) involves only s-wave pairing. However, in many ways, the Hamiltonian rather describes a p-wave superconductor due to the anomalous kinetic energy. For instance, in the vicinity of the critical lines $B = \pm\Delta$ the Hamiltonian reduces to the same Dirac Hamiltonian as the spinless p-wave superconductor. To see this, we expand the Hamiltonian about the critical point $B = \Delta$. According to Eq. (3.2), the low-energy subspace is spanned by the eigenstates of $\sigma_z\tau_x$ with eigenvalue $+1$, i.e., by

$$|+\rangle = \frac{1}{\sqrt{2}}\begin{bmatrix}1\\0\\1\\0\end{bmatrix} \qquad |-\rangle = \frac{1}{\sqrt{2}}\begin{bmatrix}0\\1\\0\\-1\end{bmatrix}. \tag{3.4}$$

Evaluating the matrix elements of H in this basis, we readily obtain the effective low-energy Hamiltonian

$$H \simeq \begin{pmatrix}\Delta - B & v_F p\\ v_F p & -(\Delta - B)\end{pmatrix}. \tag{3.5}$$

Indeed, this has the same structure as the domain-wall Hamiltonian in Eq. (2.8) for the spinless p-wave superconductor.[1] The Dirac mass is given by $\Delta - B$ which changes sign at the critical line $B = \Delta$.

For the spinless p-wave superconductor, we clearly identified one of the phases as topological while the other phase was topologically trivial. In the present case, such an identification is less obvious. In many ways, it turns out that the Δ-dominated phase is topological. However, this is not the full story. To start with, the underlying model of the topological-insulator edge has a linear spectrum, and thus no well defined vacuum (or atomic) limit which is obviously trivial. Moreover, the two phases of the proximity-coupled topological-insulator edge are related by a superconductor-magnetism duality. To see this, let us rotate the Hamiltonian (3.1) about the y-axis in spin space, such that $\sigma_x \to \sigma_z$ and $\sigma_z \to -\sigma_x$. Then, the Hamiltonian becomes

$$H = v_F p\sigma_z\tau_z + B\sigma_x + \Delta\tau_x. \tag{3.6}$$

Clearly, this Hamiltonian is invariant under the duality transformation $\tau_i \leftrightarrow \sigma_i$ and $B \leftrightarrow \Delta$ which just interchanges magnetic and superconducting quantities. This duality obviously maps the two phases into one another as the interchange $B \leftrightarrow \Delta$ changes the sign of the Dirac mass. Strictly speaking, it is thus difficult to identify one of the phases as topological.

In fact, the duality of the model has physical consequences. As shown in Ref. [22], a Josephson junction between two Δ-dominated regions with a B-dominated junction region exhibits an anomalous 4π-periodic Josephson effect. (This is discussed further

[1] Strictly speaking, this Hamiltonian involves $v_F p\tau_x$ while the corresponding Hamiltonian for the spinless p-wave superconductor involved $\Delta' p\tau_y$. These two Hamiltonians can obviously be mapped onto each other by a trivial rotation about the z-axis of particle-hole space.

in Sec. 7 below.) The magnetism-superconductivity duality implies that there is also a 4π-periodic spin Josephson effect in the inverse $B-\Delta-B$ junction arrangement when the Zeeman field points in different directions (perpendicular to the spin-orbit field) on the two sides of the junction while the superconducting phase is uniform across the junction. Note that the direction of the magnetic field in the plane perpendicular to the spin-orbit direction maps onto the superconducting phase under the duality transformation. Incidentally, this magneto-Josephson effect may be easier to observe than it might seem in that due to the spin-orbit coupling, the spin Josephson current is accompanied by a much more easily measurable charge current [23].

3.2 Zero-energy states and Majorana operators

Above, we explicitly constructed the Bogoliubov quasiparticle operator associated with the zero-energy domain wall state in spinless p-wave superconductors and showed that it is a Majorana operator satisfying $\gamma = \gamma^\dagger$. Now that we are considering more physical spinful models, it may be useful to exhibit this connection more generally.

With the convention that the Nambu spinor is ordered as $[\psi_\uparrow, \psi_\downarrow, \psi_\downarrow^\dagger, -\psi_\uparrow^\dagger]^T$, the Bogoliubov-deGennes Hamiltonian anticommutes with the product time reversal T and charge conjugation C,

$$\{H, CT\} = 0. \tag{3.7}$$

and the spectrum of H is symmetric about $E = 0$, i.e., for every eigenstate $|\psi\rangle$ with energy E, there is an eigenstate $CT|\psi\rangle$ with energy $-E$, see App. A.

Now, assume that H has a zero-energy eigenstate $|\gamma\rangle$ which is spatially isolated from any other zero-energy solution. This is exactly the situation associated with a domain wall. Since T and C are local operations, we must conclude that

$$|\gamma\rangle = CT|\gamma\rangle. \tag{3.8}$$

To see what this implies, we write the corresponding BdG spinor as $|\gamma\rangle = [\chi_e, \chi_h]^T$ where χ_e and χ_h are themselves 2-component Pauli spinors with spin-up and spin-down components. Then, the relation (3.8) implies that the electron and hole spinors are related through

$$\chi_h = T\chi_e \tag{3.9}$$

as well as $\chi_e = -T\chi_h$ (note that $T^2 = -1$). Thus, we can write the BdG spinor $|\gamma\rangle$ explicitly as

$$\langle x|\gamma\rangle = [\chi_\uparrow, \chi_\downarrow, \chi_\downarrow^*, -\chi_\uparrow^*]^T, \tag{3.10}$$

and the corresponding Bogoliubov quasiparticle operator becomes

$$\gamma = \int dx [\chi_\uparrow, \chi_\downarrow, \chi_\downarrow^*, -\chi_\uparrow^*] \cdot [\psi_\uparrow, \psi_\downarrow, \psi_\downarrow^\dagger, -\psi_\uparrow^\dagger]^T = \int dx \{\chi_\uparrow\psi_\uparrow + \chi_\downarrow\psi_\downarrow + \chi_\downarrow^*\psi_\downarrow^\dagger + \chi_\uparrow^*\psi_\uparrow^\dagger\}. \tag{3.11}$$

This operator γ clearly satisfies the Majorana relation $\gamma = \gamma^\dagger$.

4
Quantum wires

The minimal physics which turns the proximity-coupled topological insulator edge into a topological superconductor actually does not include the topological-insulator properties, but merely the fact that there is only one left-moving and one right-moving channel each. This is sufficient to emulate the spinless-fermion situation discussed in the introduction.

This point is made explicit by the quantum-wire proposal [24,25] to realize a topological superconducting phase and Majorana bound states. Let us consider a single-channel (i.e., strictly one-dimensional) quantum wire with Rashba spin-orbit coupling and applied Zeeman field B, proximity coupled to an s-wave superconductor with induced pairing Δ,

$$H = \left(\frac{p^2}{2m} + up\sigma_x - \mu \right) \tau_z - B\sigma_z + \Delta\tau_x. \tag{4.1}$$

Here, u denotes the strength of the Rashba spin-orbit coupling and we include a chemical potential μ. Importantly, the spin-orbit field, taken along the x-direction, is perpendicular to the Zeeman field, taken along the z-direction. Note that this is just the topological-insulator Hamiltonian (4.1) except for the kinetic-energy term. We will see that this term still allows topological superconducting phases, but also leads to important differences in the physics.

It is not very difficult to diagonalize and study the Hamiltonian (4.1) in full generality. However, it is perhaps more enlightening to restrict attention to limiting cases in which the physics becomes more transparent and which can be related to the models of topological superconducting phases that we have already discussed. Specifically, we consider two limits, depending on the strength of the Zeeman field relative to the spin-orbit coupling as measured by $\epsilon_{\rm so} = mu^2$, see Fig. 4.1. We will always assume that $\Delta \ll \max\{B, \epsilon_{\rm so}\}$. Then, we can consider the limits:

- Kitaev limit $B \gg \epsilon_{\rm so}$: First neglecting the spin-orbit coupling, the normal-state dispersion

  $$\epsilon_p = \frac{p^2}{2m} \pm B \tag{4.2}$$

  consists of two vertically shifted parabolas for the spin-up and spin-down electrons. The main effect of the spin-orbit coupling is that the spin polarizations of the parabolas are slightly tilted away from the Zeeman direction, with the tilt angle being proportional to p and thus having opposite signs for positive and negative momenta. Now, imagine that the chemical potential is placed below the

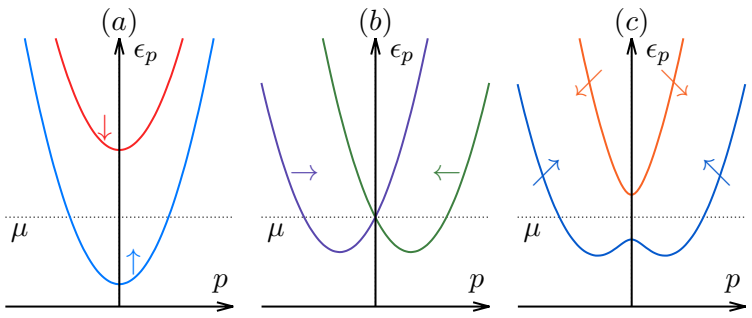

Fig. 4.1 Normal-state dispersions of the quantum wire in (a) the Kitaev limit, (b) the topological insulator limit without Zeeman field, and (c) the topological insulator limit with Zeeman field.

band bottom of the spin-down band. Then, there is only a single left-moving and a single right-moving channel (or none at all) and we will see below that this limit maps to the spinless p-wave superconductor discussed above.

- Topological-insulator limit $B \ll \epsilon_{\rm so}$: First neglecting the Zeeman field, the normal-state dispersion

$$\epsilon_p = \frac{p^2}{2m} \pm up = \frac{1}{2m}(p \pm mu)^2 - \frac{1}{2}mu^2 \tag{4.3}$$

consists of two parabolas shifted relative to each other along the momentum axis due to the Rashba spin-orbit coupling. The two parabolas correspond to spin-up and spin-down electrons with respect to the direction of the spin-orbit field (i.e., the x-direction for the Hamiltonian in Eq. (4.1)), and cross at $p = 0$. The Zeeman field applied in a direction perpendicular to the spin-orbit field (the z-direction for the Hamiltonian in Eq. (4.1)) mixes the two states at $p = 0$ and this opens a gap of size $2B$ in the spectrum, which now becomes[1]

$$\epsilon_p = \frac{p^2}{2m} \pm \sqrt{(up)^2 + B^2}. \tag{4.4}$$

When we adjust the Fermi energy to lie within this gap, we again have a situation in which there are only a single right-moving mode and a single left-moving mode at the Fermi energy. We will see that this limit is closely related to the topological-insulator model discussed in the previous section.

4.1 Kitaev limit

First consider the limit of strong Zeeman field with the Fermi energy lying far below the bottom of the spin-down parabola. In that case, we can project out the high-energy states associated with the spin-down parabola and derive an effective low-energy Hamiltonian. To do so, first neglect the spin-orbit coupling and measure the

[1]Note that the "effective Zeeman field" acting on the electron spin now has orthogonal components up from spin-orbit and B from Zeeman, i.e., the overall strength of the effective Zeeman field is $\sqrt{(up)^2 + B^2}$.

Fermi energy from the bottom of the spin-down band, i.e., shift

$$H = \left(\frac{p^2}{2m} - (B+\mu)\right)\tau_z + \text{pairing terms} \to \left(\frac{p^2}{2m} - \mu\right)\tau_z + \text{pairing terms}. \quad (4.5)$$

Now consider the pairing terms. In the absence of spin-orbit coupling, the low-energy space of the Bogoliubov-deGennes equation is spanned by the spin-up electron

$$|\mathrm{e}\rangle = [1,0,0,0]^T \quad (4.6)$$

and the spin-up hole,

$$|\mathrm{h}\rangle = [0,0,0,1]^T. \quad (4.7)$$

We can now readily see that within this subspace, there are no pairing terms. Indeed, we find that $\langle \mathrm{e}|\Delta\tau_x|\mathrm{e}\rangle = \langle \mathrm{h}|\Delta\tau_x|\mathrm{e}\rangle = \langle \mathrm{e}|\Delta\tau_x|\mathrm{h}\rangle = \langle \mathrm{h}|\Delta\tau_x|\mathrm{h}\rangle = 0$. This reflects that spin-singlet Cooper pairing cannot induce proximity superconductivity in a perfectly spin-polarized system.

To find finite pairing terms, we need to include the spin-orbit coupling. Since the latter is weak, it can be included perturbatively. Using first-order perturbation theory, spin-orbit coupling modifies the low-energy spinors into

$$|\mathrm{e}\rangle = [1, -up/2B, 0, 0]^T \quad (4.8)$$

and

$$|\mathrm{h}\rangle = [0, 0, -up/2B, 1]^T. \quad (4.9)$$

We can now repeat the calculation of the matrix elements of the pairing term within the low-energy subspace and obtain

$$\langle \mathrm{h}|\Delta\tau_x|\mathrm{e}\rangle = \langle \mathrm{e}|\Delta\tau_x|\mathrm{h}\rangle = -\frac{up}{B}\Delta \quad (4.10)$$

as well as $\langle \mathrm{e}|\Delta\tau_x|\mathrm{e}\rangle = \langle \mathrm{h}|\Delta\tau_x|\mathrm{h}\rangle = 0$. Thus, the resulting projected Hamiltonian becomes

$$H \simeq \left(\frac{p^2}{2m} - \mu\right)\tau_z - \frac{up}{B}\Delta\tau_x. \quad (4.11)$$

This is just the BdG Hamiltonian of a spinless p-wave superconductor given in Eq. (2.2). By comparing with this Hamiltonian, we see that in the Kitaev limit, the effective p-wave pairing strength of the proximity-coupled quantum wire is $\Delta'_{\text{eff}} = u\Delta/B$. The p-wave pairing is nonzero only due to the spin-orbit coupling and weakens as the Zeeman field increases and the spins become increasingly polarized. But importantly, this implies that the spin-orbit-coupled quantum wire realizes a topological superconducting phase in the limit of strong Zeeman field.

4.2 Topological-insulator limit

Now consider the opposite limit of strong spin-orbit coupling. For definiteness, let us place the chemical potential in the middle of the Zeeman-induced gap, i.e., we choose $\mu = 0$. The proximity coupling to an s-wave superconductor induces a gap Δ

in the "wings" of the spectrum, i.e., at momenta $p = \pm mu$. In contrast, there are now two mechanisms gapping out the system at $p = 0$, namely the Zeeman field and the proximity coupling. To understand the interplay of these two gapping mechanisms, we focus on small momenta where we can neglect the kinetic energy in the Hamiltonian as it is quadratic in p. Then, the quantum wire Hamiltonian (4.1) reduces to

$$H \simeq up\sigma_x\tau_z - B\sigma_z + \Delta\tau_x. \tag{4.12}$$

which is just the topological-insulator model (3.1) discussed in the previous section. Thus, the spectrum of the proximity-coupled quantum wire at small p becomes

$$E_p = \pm\sqrt{(up)^2 + (B \pm \Delta)^2}, \tag{4.13}$$

with all possible combinations of signs. As in the topological-insulator case, the gap closes for $B = \pm\Delta$, indicating a topological phase transition.

The present model has a well-defined vacuum limit, so that we can clearly identify topological and trivial phases. As we already know that the large-B limit can be mapped to a spinless p-wave superconductor, it is natural to identify the topological phase with the high-B phase with $B > \Delta$. Indeed, it is easy to check that the gap does not close when increasing the Zeeman field from the topological-insulator limit $\epsilon_{\rm so} > B$ with $B > \Delta$ to the Kitaev limit $B > \epsilon_{\rm so}$, say at fixed chemical potential $\mu = 0$, for the Hamiltonian (4.1).

The existence of two topologically distinct phases implies the existence of Majorana end states associated with domain walls. Both in the topological-insulator limit and in the Kitaev limit, their wavefunctions and Bogoliubov operators can be obtained from the same calculations which we discussed above for spinless p-wave superconductors and proximity-coupled topological insulator edges.

The closing of the gap at $B = \Delta$ implies that the small-momentum region $p \ll mu$ dominates the low-energy physics. In fact, the gap $|B-\Delta|$ at $p = 0$ is much smaller than the gap of order Δ in the wings of the spectrum at $p = \pm mu$. At first sight, one may thus be tempted that for these parameters, the physics is identical to the topological-insulator case. Actually, this is not quite correct. In many ways, the phases of the present model are exactly reversed with respect to those of the topological-insulator model! There, the 4π-periodic Josephson effect occurs for a $\Delta - B - \Delta$ arrangement. In contrast, for the quantum wire there is a 4π-periodic Josephson effect in the $B - \Delta - B$ arrangement.[2] This reversal of phases can be understood most easily in the limit of large spin-orbit energy $\epsilon_{\rm so}$ with $\mu = 0$. In this limit, the Fermi points in the wings of the spectrum are far out and essentially decoupled from the $p \simeq 0$ physics. If we now consider the two Fermi points in the wings by themselves, there is only a single right-moving and a single left-moving channel, but with proximity-induced superconducting gap. These are just the ingredients of a spinless p-wave superconductor in the topological phase! Thus, for large $\epsilon_{\rm so}$ in the topological-insulator limit, we can think of the system as a combination of a proximity-coupled topological-insulator edge and a spinless p-wave superconductor. As the latter is always topological, the overall topological Z_2 index of the quantum-wire model is just the reverse of that of the proximity-coupled topological insulator.

[2] As above, we denote the phase by B if $B > \Delta$ and vice versa.

5
Chains of magnetic adatoms on superconductors

Another proposal to realize Majorana bound states relies on a chain of magnetic impurities placed on atomically clean surfaces of conventional superconductors [26]. This system is a candidate for Majorana physics as it combines the three essential ingredients: Zeeman coupling, superconductivity, and spin-orbit coupling. The Zeeman coupling is contributed by the magnetic adatoms and the substrate provides both superconductivity and spin-orbit coupling, provided the superconductor is made of a relatively heavy element.

5.1 Shiba states

To understand this platform for topological superconductivity in more detail, we first consider the physics of individual magnetic adatoms. This is a classic problem in the theory of superconductors and was first studied in the late '60s [27–30]. It will be useful for our discussion of adatom chains to explore the physics of individual adatoms at two levels. We will see that in both descriptions, the adatom induces localized subgap states in the superconductor, referred to as Yu-Shiba-Rusinov states or Shiba states for brevity. Such subgap states in superconductors can be readily probed in STM experiments [31, 32].

5.1.1 Classical magnetic moment

The local magnetic moment of the adatoms is associated with their spin-split d-levels which will typically be far in energy from the Fermi level of the substrate superconductor. Then, the low-energy physics of the adatoms can be described in terms of its magnetic moment while its electronic degrees of freedom are effectively frozen out. The large adatom spin $\mathbf{S}$ is exchanged coupled to the electrons of the superconductor and can be approximated as classical.

The BdG Hamiltonian for a local magnetic moment in a host superconductor is given by

$$H = \left(\frac{p^2}{2m} - \mu\right)\tau_z + [V\tau_z - J\mathbf{S}\cdot\boldsymbol{\sigma}]\delta(\mathbf{r}) + \Delta\tau_x, \tag{5.1}$$

where J denotes the strength of the exchange coupling between the impurity spin located at the origin and the electrons in the superconductor. In addition to the exchange coupling, the impurity also induces potential scattering which we parametrize through its strength V. This Hamiltonian has a pair of subgap bound states localized

at the impurity site. The calculation is presented in App. C.1 and yields the symmetric bound-state energies

$$E = \pm\Delta \frac{1-\alpha^2+\beta^2}{\sqrt{(1-\alpha^2+\beta^2)^2+4\alpha^2}}, \tag{5.2}$$

where $\alpha = \pi\nu_0 SJ$ and $\beta = \pi\nu_0 V$ are dimensionless measures of the strengths of the exchange coupling and potential scattering, respectively, with ν_0 denoting the normal-state density of states of the superconductor.

These Shiba bound states possess two essential properties. First, they are *spin polarized*, with the spin pointing parallel to the direction of **S**. Second, their wave function is localized around the impurity, decaying as $1/r$ for distances r smaller than the (energy-dependent) coherence length

$$\xi_E = \frac{\hbar v_F}{\sqrt{\Delta^2 - E^2}}, \tag{5.3}$$

and exponentially beyond this length.

5.1.2 Anderson impurities

At a somewhat more refined level, we can include the electronic degrees of freedom of the adatom [33]. This description is required when the adatom d-levels are close in energy to the Fermi level of the substrate superconductor. We specifically consider a simplified model in which the magnetic adatom is a (spin-1/2) Anderson impurity, hybridized with the substrate superconductor. While this does not do full justice to the actual d-band nature of the magnetic adatoms, it captures much of the essential physics. We can follow Anderson's classic paper [34] and treat the local-moment formation within mean-field approximation.

The corresponding model Hamiltonian

$$\mathcal{H} = \mathcal{H}_d + \mathcal{H}_s + \mathcal{H}_T \tag{5.4}$$

contains a standard BCS Hamiltonian $\mathcal{H}_s$ for the host superconductor, the adatom's impurity level

$$\mathcal{H}_d = \sum_\sigma (\epsilon_d - \mu) d_\sigma^\dagger d_\sigma + U n_\uparrow n_\downarrow, \tag{5.5}$$

and its hybridization with the superconductor,

$$\mathcal{H}_T = -t \sum_\sigma [\psi_\sigma^\dagger(\mathbf{0}) d_\sigma + d_\sigma^\dagger \psi_\sigma(\mathbf{0})]. \tag{5.6}$$

Here, d_σ annihilates a spin-σ electron in the Anderson-impurity level, $n_\sigma = d_\sigma^\dagger d_\sigma$, and $\psi_\sigma(\mathbf{r})$ annihilates electrons at position $\mathbf{r}$ in the superconductor.

To analyze this Anderson model, we simplify the Hubbard term through a mean-field treatment,

$$U n_\uparrow^\dagger n_\downarrow \to \frac{U}{2} \sum_\sigma [\langle n\rangle n_\sigma - \langle m\rangle \sigma n_\sigma], \tag{5.7}$$

where we defined the occupation $n = \sum_\sigma n_\sigma$ and the site polarization $m = n_\uparrow - n_\downarrow$. The first term merely renormalizes ϵ_d. The second term introduces a local exchange

coupling in the adatom orbital.[1] If we assume that the adatom is singly occupied and develops a local moment, we have $\langle n\rangle = 1$ and $\langle m\rangle = 1$. Then, the two spin-split levels of the adatom have mean-field energies

$$E_{d\uparrow} = \epsilon_d - \mu \;\; ; \;\; E_{d\downarrow} = \epsilon_d - \mu + U, \tag{5.8}$$

where we measure these energies relative to the chemical potential μ.

Within mean-field theory, the Hamiltonian reduces to a Bogoliubov-deGennes problem which is readily solved for subgap excitations. Details of this calculation are presented in App. C.2. As for a classical magnetic moment, one finds that there is a pair of subgap excitations at energies

$$E = \pm\Delta \frac{\Gamma^2 + E_{d\uparrow}E_{d\downarrow}}{\sqrt{(\Gamma^2 + E_{d\uparrow}E_{d\downarrow})^2 + \Gamma^2(E_{d\downarrow} - E_{d\uparrow})^2}}. \tag{5.9}$$

This expression is valid for $\langle n\rangle = 1$ and $\langle m\rangle = 1$, i.e., when to a good approximation, the spin-up impurity level is occupied and the spin-down level is empty. In this limit, we can also eliminate the impurity levels by a Schrieffer-Wolf approximation and recover the description in terms of a local spin. Indeed, Eqs. (5.2) and (5.9) for the Shiba-state energies connect when identifying

$$\alpha = -\frac{\Gamma U/2}{(U/2)^2 - (\epsilon_d - \mu + U/2)^2} = -\frac{\Gamma(E_{d\uparrow} - E_{d\downarrow})}{2E_{d\uparrow}E_{d\downarrow}} \tag{5.10}$$

$$\beta = \frac{\Gamma(\epsilon_d - \mu + U/2)}{(U/2)^2 - (\epsilon_d - \mu + U/2)^2} = -\frac{\Gamma(E_{d\downarrow} + E_{d\uparrow})}{2E_{d\uparrow}E_{d\downarrow}} \tag{5.11}$$

as the dimensionless exchange and potential scattering amplitudes. More generally, the description in terms of an Anderson impurity can be made fully self consistent, describing the local-moment formation. It can also be used to calculate the relative fractions of the spectral weight of the Shiba states which are located on the impurity and in the host superconductor.

5.2 Adatom chains

Armed with this understanding of individual adatoms, we now consider chains of adatoms. For an isolated impurity, the d-levels are typically far from the Fermi level of the substrate superconductor. In a chain of adatoms, there is direct hopping between neighboring adatom orbitals and the d-levels form one-dimensional bands of adatom states. If the adatom chain is dilute, the hopping amplitude is small and the bandwidth remains negligible compared to the distance of the atomic d-levels from the Fermi energy. In this limit, illustrated in Fig. 5.1 (a) and (b), we can discuss the physics of Shiba chains at subgap energies starting from the Shiba states associated

[1] In principle, we could have also included pairing terms localized on the adatom whose strength would be determined self consistently in the presence of the coupling to the substrate superconductor. Here, we assume that the Hubbard repulsion U strongly suppresses onsite pairing effects on the adatom so that these can be neglected.

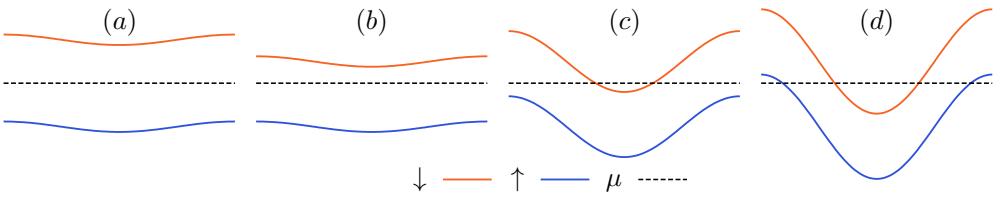

Fig. 5.1 Behavior of adatom bands for various hopping strengths w between the adatoms. As the adatom with their d-bands are modeled as Anderson impurities, there are two spin-split bands. (a) Weak hopping between Anderson-impurity states which are symmetric about the Fermi energy. In this case, the electronic degrees of freedom of the adatoms are essentially frozen out and the system can be modeled in terms of bands of Shiba states. Due to the symmetry, there is no potential scattering associated with the individual Anderson impurities. (b) Weak hopping between generic Anderson-impurity states which are asymmetric about the Fermi energy. This case can be modeled as in case (a), except that there is nonzero potential scattering associated with the individual Anderson impurities. (c) Strong hopping between Anderson impurity states such that the spin-down band crosses the Fermi energy while the spin-up band is entirely below the Fermi level. This requires that the spin-split Anderson impurity bands are asymmetric about the Fermi energy as is generically the case. This situation realizes a proximity-coupled spinless bands and is prone to develop topological superconductivity in the presence of spin-orbit coupling in the superconductor. (d) Very strong hopping between Anderson impurity states such that both spin-down and spin-up bands cross the Fermi level. As there is an even number of channels, this situation will no longer be topological.

with the individual impurities. As mentioned above, the Shiba wavefunctions decay away from the impurity only as a weak power law so that we need to account for their hybridization and the formation of Shiba bands at subgap energies of the host superconductor. The formation of Majorana bound states depends on the physics of these Shiba bands.

If, on the other hand, the adatoms are densely packed (as is presumably the case in experiment), the bandwidth of the adatom bands can exceed the energetic distance of the atomic d-levels from the Fermi level of the host superconductor. One or several adatom bands cross the superconductor's Fermi level and can no longer be treated as electronically inert. In this limit, illustrated in Fig. 5.1 (c) and (d), it is more appropriate to extend the Anderson-impurity approach for a single adatom. In fact, it is quite natural to expect topological superconductivity in this regime. Assume that we describe the adatoms as spin-1/2 Anderson impurities and assume that the adatoms spin polarize (say, into a ferromagnetic state or a spin helix). When the spin-up and spin-down levels of an individual adatom are sufficiently asymmetric about the host Fermi level, there will be a wide range of parameters where only the spin-down band crosses the Fermi level while the spin-up band is completely occupied. Notice that this is a very close realization of a spin-polarized system, and hence prone to developing effectively spinless p-wave superconductivity by proximity when there is

sufficient spin-orbit coupling in the host superconductor.[2]

We now discuss both of these scenarios in more detail.

5.2.1 Dilute adatom chains

In the dilute limit, the low-energy physics is governed by the Shiba states of the individual adatoms. In a chain of spin-polarized Shiba states, the neighboring Shiba states will couple and broaden out into subgap Shiba bands. If the Shiba states of energy $\pm E_0$ are sufficiently deep and the bandwidth sufficiently small, we can focus attention on only the Shiba states and project out the quasiparticle continua above the gap. In this limit, it is tempting to describe the Shiba chain by a Hamiltonian of the form

$$\mathcal{H} = E_0 \sum_j c_j^\dagger c_j - t \sum_j [c_{j+1}^\dagger c_j + c_j^\dagger c_{j+1}] + \Delta \sum_j [c_{j+1} c_i + c_j^\dagger c_{j+1}^\dagger]. \tag{5.12}$$

Here, we denote the fermionic annihilation (and creation) operators of the spin-polarized Shiba state at site j by c_j (and $c_j^\dagger$).[3] The Shiba states hybridize between neighboring sites with amplitude t. Moreover, the Shiba chain is embedded into the host superconductor and thus, it is natural to include a pairing term of strength Δ into this Hamiltonian. Importantly, the pairing term necessarily involves pairing correlations between different sites due to the perfect spin polarization. The Shiba states have energy $\pm E_0$ (measured from the Fermi energy).

The Hamiltonian (5.12) assumes that both hopping and pairing are dominated by nearest-neighbor terms. This is not fully adequate for a Shiba chain due to the slow $1/r$ decay of the Shiba wavefunctions away from the impurity. This has some interesting consequences, see Refs. [35,36]. Here, we restrict our discussion to the simplified model in Eq. (5.12).

The Hamiltonian (5.12) – sometimes referred to as Kitaev chain – is just a lattice version of the spinless p-wave superconductor in Eq. (2.1). We just need to identify the Shiba-state energy E_0 as playing the role of the chemical potential, $E_0 \to -\mu$. It is not difficult to diagonalize the Kitaev chain and confirm that it has a topological state at finite Δ whenever the chemical potential is situated in the normal-state band. The phase diagram of the model is shown in Fig. 5.2. For completeness, the Kitaev chain, including this phase diagram, is discussed in more detail in Sec. 5.3. Here, we continue with the discussion of the Shiba chain not to break the flow of the argument, drawing on basic aspects of the phase diagram of the Kitaev chain.

This provides the following somewhat simplified picture of Shiba chains, see Fig. 5.3. As the adatoms are placed closer together, the hybridization increases and with

[2]Spin-orbit coupling is the adatom chain would also place the system into a topological phase. However, this system has a very large Zeeman (exchange) splitting, comparable to atomic energy scales. This is presumably much larger than the spin-orbit coupling in the chain so that the induced p-wave pairing strength would be quite small, cp. Eq. (4.11). There is no such suppression when the spin-orbit coupling is provided by the host superconductor, as follows from the calculations below.

[3]The BdG Hamiltonian had two Shiba states per adatom, with energies symmetric about zero. The fact that there are two states is a consequence of the doubling of the number of degrees of freedom in the BdG formalism. This is why in the second-quantization representation of Eq. (5.12), each site supports only a single Shiba state and a single pair of annihilation and creation operators.

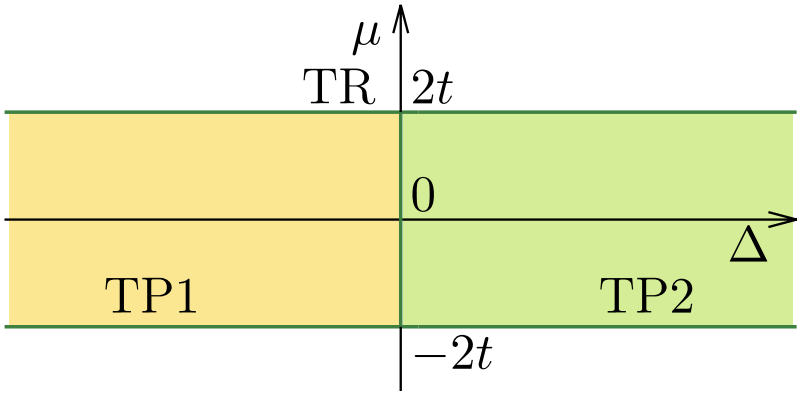

Fig. 5.2 Phase diagram of the Kitaev chain as function of p-wave pairing strength Δ and chemical potential μ. There is a topological superconducting phase when the chemical potential is within the band of the normal-state Hamiltonian, while the system is topologically trivial when the chemical potential is outside the band.

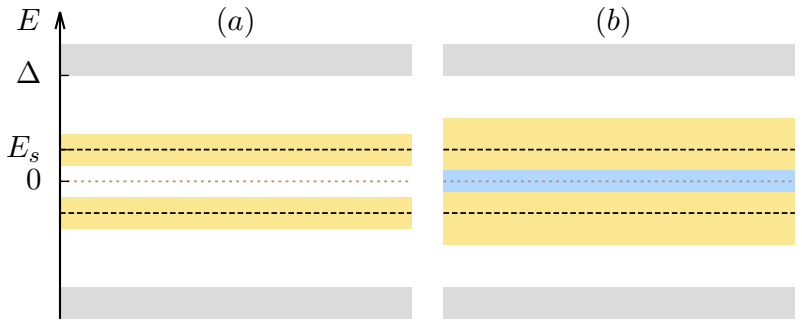

Fig. 5.3 Illustration of the subgap Shiba bands in the excitation spectrum of a dilute adatom chain. (a) For weak hybridization of deep Shiba states, the positive and negative energy Shiba bands do not cross the Fermi energy at the center of the gap and the system is nontopological. (b) For stronger hybridization, the Shiba bands overlap at the center of the gap. In this case, the pairing correlations open a gap which is of p-wave nature due to the spin polarization of the subgap states. This realizes a topological superconducting phase which hosts Majorana bound states at its ends.

it the bandwidth of the subgap Shiba bands. Initially, the Shiba bands (including the BdG partner with an energy of opposite sign) do not cross the chemical potential at the center of the gap. This is analogous to the Fermi energy lying outside the normal-state band for the Kitaev chain. Hence, the system is in a topologically trivial phase. Eventually, the two Shiba bands cross the center of the gap. Now, the pairing correlations Δ within the Shiba bands will again open a gap at the Fermi energy. This is a p-wave gap, unlike the larger gap of the host superconductor! The Shiba chain is in a topological phase and hosts zero-energy Majorana bound states at its ends.

We have simply assumed that the effective Kitaev-chain Hamiltonian for the Shiba chain contains pairing terms, but did not discuss their microscopic origin. This question is closely related to the collective behavior of the impurity spins. So far, we just noted that the Shiba states are spin polarized along the direction of the corresponding impurity spin. But we ignored the question of how the impurity spins of different adatoms are oriented with respect to one another, a question which is of obvious importance for the physics of the adatom chain. Indeed, we expect that the impurity spins interact through the familiar RKKY interaction mediated by the host superconductor and may thus order magnetically. Two such orderings have been predominantly discussed, which actually involve somewhat different physics of the pairing terms [26, 37–40].

One plausible possibility is that the chain orders ferromagnetically, with all impurity spins aligning along a certain direction. In that case, the Shiba states are all spin polarized along the same direction. This corresponds to a perfectly spin-polarized system and consequently, the spin-singlet Cooper pairs of a pure s-wave host superconductor would not be able to proximity couple to the chain of Shiba states. To induce pairing correlation within the chain of Shiba states in this case, we need to rely on (Rashba) spin-orbit coupling in the superconducting host.

An interesting alternative is the formation of a spin helix, with adatom spins rotating along the chain. In this case, neighboring impurity spins are not aligned and the corresponding Shiba states are polarized along different directions. A spin singlet Cooper pair of the host superconductor can effectively tunnel into the chain as long as its spin-up and spin-down electrons enter on different sites of the chain. Thus, the effective pairing correlations which result from these processes are just of the spinless p-wave type which are included in the Kitaev chain (5.12).

In the remainder of this section, we will assume that the adatom spins order ferromagnetically as suggested by experiment. However, it is useful to make two comments: (i) The assumption of ferromagnetic order combined with (Rashba) spin-orbit coupling in the host superconductor is less restrictive that it may appear. The reason is that this situation can be mapped on a Hamiltonian with helical spin ordering by a simple unitary transformation [41]. (ii) The stability of ordering in one dimension is obviously subtle. It depends on specifics of the microscopic Hamiltonian such as the presence or absence of continuous spin symmetries or the range of the substrate-induced interaction between adatom spins. Thermal fluctuations may well preclude long-range spin order. In that case, we assume that there is at least short range order on a scale which is large compared to the length of the adatom chains.

5.2.2 Dense adatom chains

We now consider the situation when hopping between the Anderson impurity levels of neighboring adatoms is sufficiently strong so that the spin-down band crosses the Fermi energy. At the same time, the spin-up band is fully occupied. We further assume that the adatom chain is ferromagnetically ordered, as observed in experiment [15]. In this chapter, we show that this system is prone to be in a topological superconducting phase. A more complete theoretical treatment along these lines can be found in the literature [42].

To understand the low-energy physics in this limit, it is sufficient to consider the spin-down band which crosses the Fermi level. In the vicinity of the Fermi energy, we can linearize its dispersion so that the main characteristics are its Fermi wavevector k_0 and Fermi velocity v_F. A subgap excitation in this band cannot decay into the superconducting host due to the superconducting gap, but some of its spectral weight will be transfered. In the absence of spin-orbit coupling, the superconducting substrate will not be able to induce a gap within this spin-polarized band, but there can be p-wave-like correlations in the presence of spin-orbit coupling. These superconducting correlations can be read off from the Green function for the adatom bands once we account for the coupling to the superconductor through the appropriate self energy. The self energy can be computed exactly when treating the onsite Hubbard term in mean-field theory and assuming ferromagnetic order of the chain from the outset.

The Bogoliubov-deGennes Hamiltonian of the adatom chain on top of a spin-orbit coupled s-wave superconductor can be written as

$$H = \begin{pmatrix} H_s & H_T \\ H_T^T & H_d \end{pmatrix}. \tag{5.13}$$

Here, the adatoms are described as a chain of Anderson impurities, i.e., a Hamiltonian H_d with matrix elements

$$H_d^{ij} = \left[(\epsilon_d - \mu)\delta_{ij} - W_{ij}\right]\tau_z - B\sigma_z\delta_{ij} \tag{5.14}$$

$$\tag{5.15}$$

in site space. We have already used a mean-field decoupling of the onsite Hubbard terms which results in the exchange field B governing the spin splitting. The principal new ingredient compared to the individual adatom is the direct hopping term

$$W_{ij} = -w(\delta_{i,j+1} + \delta_{i,j-1}) \tag{5.16}$$

between adatom orbitals, which leads to the formation of the adatom spin-up and spin-down bands with band width $2w$. As usual, τ_i and σ_i with $i = x, y, z$ are Pauli matrices in Nambu and spin space. We choose the chain to be aligned along the x-direction.

The host superconductor obeys the Bogoliubov-deGennes Hamiltonian

$$H_s = \left[\frac{(\mathbf{p} + k_h\sigma_x\hat{x})^2}{2m} - \mu\right]\tau_z + \Delta\tau_x. \tag{5.17}$$

Here, Δ is the superconducting order parameter and k_h denotes the strength of spin-orbit coupling. We make no attempt at a microscopic description of the spin-orbit coupling appropriate for real materials, but rather retain only the relevant term needed for inducing p-wave pairing in the adatom chain. This term couples spin to the momentum along the adatom chain. The adatoms hybridize with the superconductor through H_T which includes tunneling amplitudes t between the adatom impurity level and the superconductor at the positions $\mathbf{R}_j = ja\hat{\mathbf{x}}$ of the impurities. (a is the lattice spacing along the chain direction).

We denote the Green function of the adatom chain before and after coupling to the superconductor by $g_d(E)$ and $G_d(E)$, respectively. These two Green functions are related by the Dyson equation

$$G_{d,ij}(E) = g_{d,ij}(E) + \sum_{mn} g_{d,im}(E)\Sigma_{d,mn}(E)G_{d,nj}(E). \tag{5.18}$$

where m, n, i, j are site indices along the chain and $\Sigma_d(E)$ is the self energy accounting for the coupling to the superconductor,

$$\Sigma_{mn}(E) = t^2 \tau_z g_{s,mn}(E) \tau_z. \tag{5.19}$$

This self energy describes hopping from the chain into the superconductor and back, with free propagation in the superconductor in between, as described by the Green function $g_{s,mn}(E)$.

The Green function of the superconductor is readily computed. First consider off-diagonal elements in site space, $m \neq n$. Then

$$\begin{aligned}
g_{s,mn}(E) &= \langle \mathbf{R}_m | (E - H_s)^{-1} | \mathbf{R}_n \rangle \\
&= \langle \mathbf{R}_m | \left[E - \left(\frac{(\mathbf{p} + k_h a \sigma_x \hat{x})^2}{2m} - \mu \right) \tau_z - \Delta \tau_x \right]^{-1} | \mathbf{R}_n \rangle \\
&= \langle \mathbf{R}_m | e^{-ik_h x \sigma_x} \left[E - \left(\frac{\mathbf{p}^2}{2m} - \mu \right) \tau_z - \Delta \tau_x \right]^{-1} e^{ik_h x \sigma_x} | \mathbf{R}_n \rangle \\
&= e^{-ik_h(m-n)a\sigma_x} \frac{1}{V} \sum_{\mathbf{k}} \frac{e^{i\mathbf{k}\cdot(\mathbf{R}_m - \mathbf{R}_n)}}{E - \xi_k \tau_z - \Delta \tau_x} \\
&= e^{-ik_h(m-n)a\sigma_x} \left[(E + \Delta\tau_x) P_0(|m-n|a) + \tau_z P_1(|m-n|a) \right].
\end{aligned} \tag{5.20}$$

Here, we introduced the integrals

$$P_0(r) = \frac{\nu_0}{2} \int d\xi_k \int_{-1}^{1} dx \, \frac{e^{ikrx}}{E^2 - \xi_k^2 - \Delta^2} = -\frac{\pi \nu_0}{\sqrt{\Delta^2 - E^2}} \frac{\sin k_F r}{k_F r} e^{-r/\xi_E} \tag{5.21}$$

$$P_1(r) = \frac{\nu_0}{2} \int d\xi_k \int_{-1}^{1} dx \, \frac{\xi_k e^{ikrx}}{E^2 - \xi_k^2 - \Delta^2} = -\pi \nu_0 \frac{\cos k_F r}{k_F r} e^{-r/\xi_E} \tag{5.22}$$

with $\xi_E = \hbar v_F / \sqrt{\Delta^2 - E^2}$. An explicit evaluation of these integrals can be found in App. A of Ref. [35]. Then, we obtain

$$g_{s,mn}(E) = -\pi \nu_0 e^{-ik_h x_{mn} \sigma_x} \left\{ \frac{E + \Delta\tau_x}{\sqrt{\Delta^2 - E^2}} \frac{\sin k_F r_{mn}}{k_F r_{mn}} e^{-r_{mn}/\xi_E} + \tau_z \frac{\cos k_F r_{mn}}{k_F r_{mn}} e^{-r_{mn}/\xi_E} \right\} \tag{5.23}$$

with $x_{mn} = x_m - x_n = (m-n)a$ and $r_{mn} = |x_{mn}|$. An analogous calculation for the diagonal elements in site space, $m = n$, yields [see also Eq. (C.17)]

$$g_{s,mm}(E) = -\pi \nu_0 \frac{E + \Delta\tau_x}{\sqrt{\Delta^2 - E^2}}. \tag{5.24}$$

Thus, the self-energy takes the form

$$\Sigma_{d,mn}(E) = \begin{cases} -\Gamma \frac{E-\Delta\tau_x}{\sqrt{\Delta^2-E^2}} & m=n \\ \frac{-\Gamma}{k_F r_{mn}} e^{-ik_h x_{mn}\sigma_x} e^{-r_{mn}/\xi_E} \left[\frac{E-\Delta\tau_x}{\sqrt{\Delta^2-E^2}} \sin k_F r_{mn} + \tau_z \cos k_F r_{mn} \right] & m \neq n \end{cases} \tag{5.25}$$

This result for the self energy has several important physical consequences as we will discuss in the following.

In general, the self energy is a 4×4-matrix in Nambu and spin space,

$$\Sigma_d(E) = \begin{pmatrix} \Sigma^{ee}_{\uparrow\uparrow} & \Sigma^{ee}_{\uparrow\downarrow} & \Sigma^{eh}_{\uparrow\downarrow} & \Sigma^{eh}_{\uparrow\uparrow} \\ \Sigma^{ee}_{\downarrow\uparrow} & \Sigma^{ee}_{\downarrow\downarrow} & \Sigma^{eh}_{\downarrow\downarrow} & \Sigma^{eh}_{\downarrow\uparrow} \\ \Sigma^{he}_{\downarrow\uparrow} & \Sigma^{he}_{\downarrow\downarrow} & \Sigma^{hh}_{\downarrow\downarrow} & \Sigma^{hh}_{\downarrow\uparrow} \\ \Sigma^{he}_{\uparrow\uparrow} & \Sigma^{he}_{\uparrow\downarrow} & \Sigma^{hh}_{\uparrow\downarrow} & \Sigma^{hh}_{\uparrow\uparrow} \end{pmatrix} \tag{5.26}$$

where each block is still a matrix in site space. In the absence of spin-orbit coupling, the self energy decomposes into two independent 2×2-blocks, as several matrix elements vanish,

$$\Sigma_d(E) = \begin{pmatrix} \Sigma^{ee}_{\uparrow\uparrow} & 0 & \Sigma^{eh}_{\uparrow\downarrow} & 0 \\ 0 & \Sigma^{ee}_{\downarrow\downarrow} & 0 & \Sigma^{eh}_{\downarrow\uparrow} \\ \Sigma^{he}_{\downarrow\uparrow} & 0 & \Sigma^{hh}_{\downarrow\downarrow} & 0 \\ 0 & \Sigma^{he}_{\uparrow\downarrow} & 0 & \Sigma^{hh}_{\uparrow\uparrow} \end{pmatrix}. \tag{5.27}$$

The diagonal entries in particle-hole space describe the renormalization of the quasiparticle weight and the dispersion while the off-diagonal entries describe the proximity-induced s-wave correlations. This is considered in more detail in App. B.

For the ferromagnetically-ordered adatom chain, we assumed that only the spin-down band crosses the Fermi energy. For a description of the low-energy physics, we can therefore project the Green functions and the self energy onto this subspace, e.g.,

$$\Sigma_d(E) \to \begin{pmatrix} \Sigma^{ee}_{\downarrow\downarrow} & \Sigma^{eh}_{\downarrow\downarrow} \\ \Sigma^{he}_{\downarrow\downarrow} & \Sigma^{hh}_{\downarrow\downarrow} \end{pmatrix}. \tag{5.28}$$

The diagonal entries describe the renormalization of the quasiparticle weight and the dispersion of the spin-down band while the off-diagonal entries describe the proximity-induced pairing correlations. As these pairing correlations are induced in a spin-polarized band, they require nonzero spin-orbit coupling. They are necessarily of p-wave nature and thus odd in momentum as well as off-diagonal in site space.

In the original 4×4-scheme, the p-wave pairing terms correspond to the $\tau_x\sigma_x$ entries. Moreover, we focus on subgap energies, $E \ll \Delta$. Then, the projected self energy takes the explicit form

$$\Sigma_{d,mn}(E) \simeq -\frac{\Gamma E}{\Delta}\delta_{mn} - i\frac{\Gamma e^{-r_{mn}/\xi_0}}{k_F r_{mn}} \sin k_h x_{mn} \sin k_F r_{mn} \tau_x (1-\delta_{mn}). \tag{5.29}$$

This is already written in the 2×2- matrix notation after projection, where $\tau_x\sigma_x$ becomes τ_x. The first term renormalizes the band dispersion while the second describes

the induced p-wave pairing. Note that it is indeed odd in site space as expected for p-wave correlations and vanishes in the absence of spin-orbit coupling, i.e., when $k_h = 0$. Here, we will not pursue a detailed evaluation of these pairing correlations, but simply assume that they are finite,

$$\Sigma_{d,mn}(E) \simeq -\frac{\Gamma E}{\Delta}\delta_{mn} + \Delta_{mn}\tau_x, \tag{5.30}$$

The interested reader can find a more complete discussion in Ref. [42].

Then, the Dyson equation for the projected Green function in momentum space becomes

$$G_d^{-1}(k,E) \simeq E(1+\Gamma/\Delta) - v_F(k-k_0)\tau_z + \Delta(k)\tau_x, \tag{5.31}$$

where we explicitly linearized the dispersion of the spin-down band and $\Delta(k)$ denotes the Fourier transform of Δ_{mn} to momentum space. Besides the induces p-wave correlations, this expression includes a strong renormalization of the quasiparticle weight when $\Gamma \gg \Delta$. Indeed, Γ measures the strength of hybridization between adatoms and superconductor. In adatom experiments, this coupling is essentially determined by atomic physics and expected to be large compared to the gap. In this situation, excitations in the adatom band will have much spectral weight in the superconductor, leading to a strong renormalization of the quasiparticle weight,

$$Z = \frac{1}{1+\Gamma/\Delta}. \tag{5.32}$$

This renormalization affects the dispersion and the induced gap of the adatom band at subgap energies,

$$G_d(k,E) \simeq \frac{Z}{E - Zv_F(k-k_0)\tau_z + Z\Delta(k)\tau_x}. \tag{5.33}$$

We observe that the effective Fermi velocity is strongly renormalized,

$$v_F \to \tilde{v}_F = Zv_F. \tag{5.34}$$

Loosely speaking, this renormalization can be understood by noting that the excitations "spend little time" in the wire and propagate along the wire only during these intervals. Indeed, to a good approximation, the non-pairing contributions to the self energy are local in site space. Similarly, the physical induced gap involves the same renormalization factor,

$$\Delta_{\text{ind}} = Z|\Delta(k_0)|. \tag{5.35}$$

Notice, however, that $\Delta(k)$ is itself proportional to the large coupling Γ, making Δ_{ind} independent of Γ at strong coupling.

This renormalization is confirmed [42] by more detailed calculations of the subgap spectrum for all momenta k. The results of such a calculation are shown in Fig. 5.4(a). The figure shows the original dispersion of the adatoms as black dashed lines while the true dispersion accounting for the coupling to the superconductor is shown

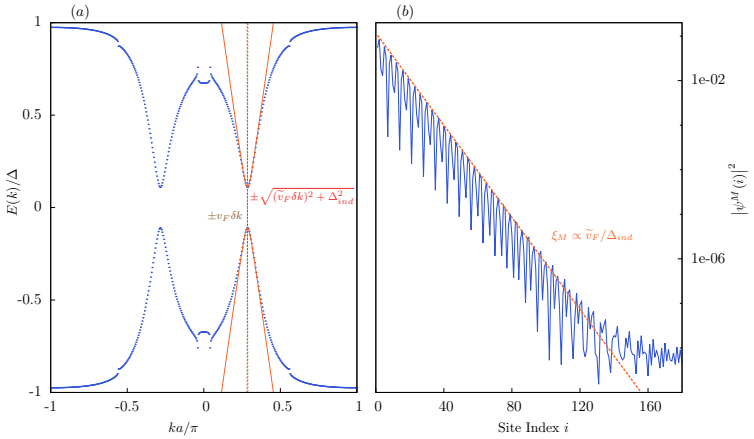

Fig. 5.4 (a) Excitation spectrum of a dense adatom chain coupled to a host superconductor. Only the spin-down adatom band (shown by the black dashed lines) crosses the Fermi level. The subgap dispersion accounting for the coupling to the superconductor is shown as a full, blue line. The approximate theory presented in the text is shown in red and accurately reproduces the numerically exact results near the Fermi wavevector of the adatom band. Note the strong renormalization of the Fermi velocity compared to the bare dispersion as well as the proximity-induced p-wave gap. (b) Numerically exact results for a Majorana wavefunction, showing that it is localized on a scale which is small compared to the coherence length of the host superconductor.

in blue. These dispersion curves exhibit the minimal gap at the wavevector k_0 where the adatom band crosses the Fermi energy, but the slopes are dramatically reduced in accordance with the downward renormalization of the Fermi velocity. Indeed, we can quantitatively compare these exact excitation spectra with the results of the approximate theory presented here. Eq. (5.33) predicts a low energy dispersion

$$E_k = \pm\sqrt{(Zv_F(k-k_0))^2+\Delta_{\rm ind}^2}, \tag{5.36}$$

which is shown in red in Fig. 5.4(a).

The most important consequence of this renormalization concerns the localization length of the Majorana bound states. We can extract a characteristic length from Eq. (5.36), which is given by

$$\xi_M = Z\frac{\hbar v_F}{\Delta_{\rm ind}}. \tag{5.37}$$

This length describes the coherence length of the induced superconducting correlations. It is important to note that due to the renormalization of the Fermi velocity, this can be significantly smaller than the coherence length of the host superconductor, $\xi = \hbar v_F/\Delta$. This is important because ξ_M also governs the localization of the Majorana end states. The Majorana states can thus be much more strongly localized than the coherence length of the host superconductor when the coupling to the superconductor is strong! This might have been observed in a recent experiment [15]. This scenario

for the Majorana localization length is also confirmed by more detailed numerical calculations, as illustrated in Fig. 5.4(a).

5.3 Insert: Kitaev chain

5.3.1 Finite chain and Majorana end states

Let us first consider

$$\mathcal{H} = -t\sum_j [c_{j+1}^\dagger c_j + c_j^\dagger c_{j+1}] + \Delta \sum_j [c_{j+1} c_i + c_j^\dagger c_{j+1}^\dagger] - \mu \sum_j c_j^\dagger c_j \tag{5.38}$$

(i.e., the Hamiltonian in Eq. (5.12) with the replacement $E_0 \to -\mu$) for a finite chain of N sites [18]. It turns out that there is a particularly simple and instructive solution of the finite chain for the special point $t = \Delta$ and $\mu = 0$. We start by writing the fermionic operator

$$c_j = \frac{1}{2}(\gamma_{Bj} + i\gamma_{Aj}), \tag{5.39}$$

in terms of two Majorana operators γ_{Aj} and γ_{Bj} with $\gamma_{Aj} = \gamma_{Aj}^\dagger$ and $\gamma_{Bj} = \gamma_{Bj}^\dagger$. Using the inverse relations $\gamma_{Aj} = -i[c_j - c_j^\dagger]$ and $\gamma_{Bj} = c_j + c_j^\dagger$ as well as the usual fermionic anticommutation relations for c_j, one easily checks that the operators γ_{Aj} and γ_{Bj} do indeed satisfy the Majorana relation in Eq. (1.3). We can now express the Hamiltonian in terms of these new operators. At the special point, this yields

$$\mathcal{H} = -it\sum_{j=1}^{N-1} \gamma_{Bj}\gamma_{A,j+1}. \tag{5.40}$$

This Hamiltonian can be diagonalized by introducing $N-1$ new (conventional) fermionic operators through

$$d_j = \frac{1}{2}(\gamma_{Bj} - i\gamma_{A,j+1}), \tag{5.41}$$

for $j = 1, \ldots N-1$. Note that these new operators combine Majorana operators which derive from neighboring sites. If we now express the Hamiltonian in terms of these new operators, we find

$$\mathcal{H} = 2t\sum_{j=1}^{N-1} \left(d_j^\dagger d_j - \frac{1}{2} \right). \tag{5.42}$$

Thus, the d_j are fermionic quasiparticle (Bogoliubov) operators of the superconductor with energy t.

It is important to realize that we started with N fermionic operators c_j. In contrast, we seem to have only $N-1$ quasiparticle operators d_j. Where did we lose one of the fermionic operators? If we look back at the Hamiltonian (5.40) written in terms of the Majorana operators, we realize that two of the Majorana operators actually neither appear in the Hamiltonian nor in the quasiparticle operators d_j, namely γ_{A1} and γ_{BN}!

To understand what this means, we note that these operators commute with the Hamiltonian $\mathcal{H}$. Thus, they are eigenoperators of the Hamiltonian with *zero* energy.

There is one such zero-energy Majorana excitation localized at each end of the chain. We can combine these two Majorana operators into an additional (highly-nonlocal) conventional fermion,

$$d_0 = \frac{1}{2}(\gamma_{BN} - i\gamma_{A1}). \tag{5.43}$$

This fermionic operator does not appear in the Hamiltonian and thus has zero energy. Assume that we find a many-body ground state $|\mathrm{gs}\rangle$ of the chain with the additional condition $d_0|\mathrm{gs}\rangle = 0$. Then, there is necessarily a second ground state

$$d_0^\dagger|\mathrm{gs}\rangle. \tag{5.44}$$

Indeed, since the quasiparticle excitation generated by $d_0^\dagger$ has zero energy, this state has exactly the same energy as $|\mathrm{gs}\rangle$. Thus, we find that the ground state of a finite Kitaev chain is doubly degenerate and that this degeneracy is associated with the existence of Majorana end states at the two ends of the chain.

5.3.2 Bulk properties and phase diagram

To compute the bulk properties of the Kitaev chain for arbitrary parameters, we consider the Hamiltonian (5.38) for N sites with periodic boundary conditions, i.e., we identify

$$c_1 = c_{N+1}. \tag{5.45}$$

By translational invariance, this can be diagonalized by introducing a_k through

$$c_j = \frac{1}{\sqrt{N}} \sum_j e^{ikj} a_k. \tag{5.46}$$

Indeed, this yields

$$\mathcal{H} = \sum_k \xi_k a_k^\dagger a_k + \Delta \sum_k [e^{ik} a_k a_{-k} + e^{-ik} a_{-k}^\dagger a_k^\dagger], \tag{5.47}$$

where

$$\xi_k = -2t \cos k - \mu \tag{5.48}$$

is the normal-state dispersion.

To find the quasiparticle spectrum, we pass to Nambu space by introducing the two-component Nambu operator

$$\phi_k = \begin{pmatrix} a_k \\ a_{-k}^\dagger \end{pmatrix}. \tag{5.49}$$

Note that we define ϕ_k for $k > 0$ only to avoid double counting.[4] Indeed, if one remembers this condition, it is straight-forward to show that the ϕ_k satisfy the usual fermionic anticommutation relations,

$$\{\phi_{k\alpha}, \phi_{k'\alpha'}^\dagger\} = \delta_{kk'}\delta_{\alpha\alpha'}$$

[4] We can leave out the $k = 0$ term as there is no pairing term in this case.

$$\{\phi_{k\alpha}, \phi_{k'\alpha'}\} = 0 \tag{5.50}$$
$$\{\phi^\dagger_{k\alpha}, \phi^\dagger_{k'\alpha'}\} = 0.$$

We can now write the Hamiltonian as

$$\mathcal{H} = \sum_{k>0} \phi^\dagger_k H_k \phi_k + \text{const} \tag{5.51}$$

with the Bogoliubov-deGennes (BdG) Hamiltonian

$$H_k = \begin{pmatrix} \xi_k & 2i\Delta \sin k \\ -2i\Delta \sin k & -\xi_k \end{pmatrix}. \tag{5.52}$$

Note that the off-diagonal terms in the BdG Hamiltonian are odd functions of k which is a direct signature of the p-wave nature of the pairing. We can now obtain the excitation spectrum

$$E_k = \pm\sqrt{\xi_k^2 + 4\Delta^2 \sin^2 k} \tag{5.53}$$

in the usual way by diagonalizing the BdG Hamiltonian.

The connection with the the continuum model for spinless p-wave superconductor (see Sec. 2.1) is readily made explicit. Consider a Fermi energy close to the lower band edge so that the relevant wavevectors are small. Then we can expand both the dispersion ξ_k and the pairing $\Delta \sin k$ for small k. In this limit, we simply recover both the BdG Hamiltonian (2.2) and the spectrum (2.3) for the spinless p-wave superconductor.

The excitation spectrum (5.53) of the Kitaev chain is mostly fully gapped. The normal-state dispersion ξ_k vanishes only for $k = \pm k_F$ where the Fermi wavevector k_F is determined by the condition $-2t \cos k_F = \mu$. Similarly, the pairing term is nonzero except when $k = 0$ and $k = \pm\pi$. Thus, the system becomes gapless only when the Fermi wavevector becomes equal to 0 or $\pm\pi$. This happens when the chemical potential is just at the band edges of the normal-state dispersion, i.e., when $\mu = -2t$ ($k_F = 0$) or $\mu = +2t$ ($k_F = \pm\pi$).

The lines $\mu = \pm 2t$ where the excitation spectrum becomes gapless correspond to phase boundaries between two topologically distinct phases. The corresponding phase diagram as a function of Δ and μ (both measured in units of t) is shown in Fig. 5.2. The Kitaev chain is in a topological phase when the chemical potential lies within the band of the normal-state band. Conversely, the system becomes topologically trivial when the chemical potential is outside the band. In the latter case, the system is adiabatically connected to the vacuum ($\mu \to -\infty$) or a fully occupied band ($\mu \to \infty$). The special point $t = \Delta$ and $\mu = 0$ discussed above is well within the topological phase.

6
Nonabelian statistics

Perhaps the most fascinating property of Majorana zero modes is their nonabelian quantum statistics. Nonabelian statistics of Majorana zero modes was first discussed in two-dimensional systems where Majoranas appear as zero-energy bound states associated with vortices in spinless $p + ip$ superconductors [43–45]. At first sight, it might not be obvious whether Majoranas in one-dimensional systems as discussed here would also obey the same quantum statistics. In fact, the Majoranas in 1d are associated with domain walls rather than vortices, while physical arguments for nonabelian statistics in 2d rely heavily on the phase structure of the order parameter associated with a vortex. More generally, quantum statistics is not well defined in strictly one-dimensional systems as exchanging particles cannot be disentangled from interactions as the particles necessarily pass one another in the exchange process (or formally, one can pass between, e.g., boson and fermion representations by means of a Jordan-Wigner transformation). The second point can be readily circumvented by considering wire networks rather than strictly one-dimensional systems [46].

6.1 Manipulation of Majorana bound states

A necessary prerequisite for probing nonabelian statistics of Majorana zero modes in experiment is the ability to manipulate the Majorana zero modes. The most direct way of performing braiding operations is by explicitly moving the Majorana states in real space. Using the quantum-wire scenario as an example, let us briefly discuss how this might be achieved in practice. To move the Majorana zero mode along the wire, we need to move the domain wall with which it is associated. As we saw in Sec. 4, we can induce the domain wall by spatially varying parameters in such a way that the topological gap changes sign.

Consider first the Kitaev limit of the quantum-wire Hamiltonian (4.1), i.e., the limit of large Zeeman splitting. In this limit, the topological phase transition occurs when the chemical potential moves through the bottom of the band, and in the vicinity of the phase transition, the gap is given by the chemical potential μ. Thus, we can tune through the phase transition by changing the chemical potential, and induce a domain wall by changing the chemical potential along the wire. This can in principle be achieved by changing the local electrostatic potential through a series of gate electrodes along the wire.

Next consider the topological-insulator limit of the quantum wire Hamiltonian (4.1). In Sec. 4, we considered the case of zero chemical potential, $\mu = 0$. In that case, the topological gap is given by the difference of Zeeman field and gap, $B - \Delta$. While in principle, B and Δ can be varied along the wire, these are not conveniently

controlled experimentally. It turns out that also in this limit, we can tune through the transition by varying the chemical potential. Indeed, one can solve for the spectrum of Hamiltonian (4.1) in this limit at finite chemical potential by squaring the Hamiltonian, along the same lines as described in Sec. 4. In this way, one finds that the gap is given by

$$B - \sqrt{\Delta^2 + \mu^2}. \tag{6.1}$$

This shows that can again change the topological gap by tuning μ [46].

An alternative method relies on changing the superconducting order parameter of the proximity-coupled superconductor [47]. While it may be inconvenient to change the magnitude of Δ, the phase of the order parameter is readily manipulated. Indeed, there is a phase gradient associated with a supercurrent flowing along the superconductor. Incorporating this phase gradient into Hamiltonian (4.1), one readily finds that the phase boundary between topological and nontopological phase depends on the phase gradient. In fact, it turns out that in quantum wires in the topological-insulator limit, a finite phase gradient pushes the system towards the topological phase. In this limit, the topological gap is given by $B - \Delta$. Roughly, the effect of the supercurrent can be viewed as reducing the superconducting correlations, pushing the system towards the topological phase. As a result, one can induce Majorana-carrying domain walls in the quantum wires by having supercurrents of different strengths flowing along different segments of the wire. These domain walls can be moved by changing these supercurrents as function of time.

Based on such methods of manipulating domain walls, one can explicitly establish the nonabelian statistics of the Majorana bound states within the quantum-wire platform [46]. Below, we will see that in principle, Majoranas can also be effectively braided merely by varying the pairwise couplings between a number of Majoranas on a Y-junction [48]. These couplings can be manipulated, e.g., by moving pairs of Majoranas closer together, increasing their spatial overlap, or by changing the magnitude of the topological gap in between, affecting the localization length and hence the spatial overlap. Another interesting method relies on charging physics [49].

6.2 Insert: Nonabelian Berry phase

The basis for analyzing the braiding of Majorana bound states is the nonabelian Berry phase. An essential assumption in the standard derivation of the Berry phase [50] is that the instantaneous spectrum is nondegenerate at all times. The existence of zero-energy Majorana modes implies that the ground state is degenerate and this degeneracy persists during the entire braiding process. The adiabatic evolution in the presence of degeneracies was first analyzed by Wilczek and Zee [51] in a classic paper. They find that in this case, the adiabatic dynamics is not simply described by a geometric phase associated with a conventional vector potential (Berry connection) but rather with a geometric unitary transformation on the subspace of degenerate states which can be expressed in terms of a nonabelian vector potential or Berry connection. This is sometimes referred to as nonabelian Berry phase. For completeness, we briefly recapitulate the derivation of the nonabelian Berry phase as it provides the basis for describing a simple model for the braiding of Majorana zero modes in the next section.

Consider a Hamiltonian $H(\boldsymbol{\lambda}(t))$ which depends on time through a set of parameters $\boldsymbol{\lambda} = (\lambda_1, \lambda_2, \ldots)$, with the instantaneous spectrum

$$H(\boldsymbol{\lambda}(t))|\psi_\alpha^n(t)\rangle = E_n(t)|\psi_\alpha^n(t)\rangle. \tag{6.2}$$

This spectrum contains one or several subsets n of degenerate states. The states within each of these degenerate subspaces of dimension d_n are labeled by $\alpha = 1, \ldots, d_n$. Let us now define the adiabatic solution of the corresponding time-dependent Schrödinger equation

$$i\partial_t|\eta_\alpha^n(t)\rangle = H(\boldsymbol{\lambda}(t))|\eta_\alpha^n(t)\rangle. \tag{6.3}$$

with initial condition

$$|\eta_\alpha^n(t=0)\rangle = |\psi_\alpha^n(t=0)\rangle. \tag{6.4}$$

In the adiabatic limit, the time evolution does not take the system out of the degenerate subspace to which the initial state belongs. But unlike in the nondegenerate case, the time-evolved state need not remain parallel to $|\psi_\alpha^n(t)\rangle$ at later times. Instead, the time-evolved state can be a linear combination of all the states within the degenerate subspace,

$$|\eta_\alpha^n(t)\rangle = \sum_{\beta=1}^{d_n} U_{\alpha\beta}^n(t)|\psi_\beta^n(t)\rangle. \tag{6.5}$$

Note that the $U_{\alpha\beta}^n(t)$ are just prefactors in a linear combination and not Hilbert-space operators.

To deduce the $U_{\alpha\beta}^n(t)$, we insert this expansion into the time-dependent Schrödinger equation which yields

$$i\sum_\beta [\partial_t U_{\alpha\beta}^n(t)]|\psi_\beta^n(t)\rangle + i\sum_\beta U_{\alpha\beta}^n(t)|\partial_t\psi_\beta^n(t)\rangle = E_n(t)\sum_\beta U_{\alpha\beta}^n(t)|\psi_\beta^n(t)\rangle. \tag{6.6}$$

Multiplying this equation from the left by $\langle\psi_\gamma^n(t)|$ and dropping the subspace index n for simplicity of notation, we find

$$i\partial_t U_{\alpha\gamma} + i\sum_\beta U_{\alpha\beta}\langle\psi_\gamma|\partial_t\psi_\beta\rangle = EU_{\alpha\gamma}. \tag{6.7}$$

We can now define the nonabelian Berry connection

$$A_{\alpha\beta}(t) = i\langle\psi_\beta|\partial_t\psi_\alpha\rangle \tag{6.8}$$

so that we obtain, in matrix notation,

$$i\partial_t U = U(E - A). \tag{6.9}$$

Note that this equation has the same structure as the Schödinger equation of the time-evolution operator for a time-dependent Hamiltonian, except that on the right-hand side, the analog of the Hamiltonian stands to the right of the time-evolution operator. Thus, as is familiar from the time-evolution operator, this equation can be solved

formally in terms of the anti-time-ordering operator $\tilde{T}$ which orders factors according to ascending time from left to right. Thus, we find the explicit solution

$$U^n(t) = e^{-i\int_0^t dt' E_n(t')} \tilde{T} e^{i\int_0^t dt' A^n(t')}, \tag{6.10}$$

where we have restored the subspace index n.

To bring out the geometric nature of the time evolution, we can introduce a nonabelian vector potential which replaces time derivatives by derivatives with respect to the parameters λ_j,

$$\mathbf{A}^n_{\alpha\beta}(t) = i\langle\psi^n_\beta|\nabla_{\boldsymbol{\lambda}}\psi^n_\alpha\rangle. \tag{6.11}$$

Then, U^n can be written in terms of an anti-path-ordered integral in parameter space,

$$U^n(t) = e^{-i\int_0^t dt' E_n(t')} \tilde{P} e^{i\int d\boldsymbol{\lambda}\cdot\mathbf{A}^n(\boldsymbol{\lambda})}. \tag{6.12}$$

The path-ordered exponential of the nonabelian vector potential generalizes the familiar Berry phase. It only depends on the path in parameter space, not on the way in which the path is being traversed, and is a purely geometric object. Now, we can also express the time-evolution operator

$$\mathcal{U}(t) \simeq \sum_n \sum_\alpha |\eta^n_\alpha(t)\rangle\langle\eta^n_\alpha(0)| = \sum_n \sum_{\alpha\beta} U^n(t)|\eta^n_\beta(t)\rangle\langle\psi^n_\alpha(0)| \tag{6.13}$$

within the adiabatic approximation.

Finally, we briefly discuss how the vector potential transforms under a change of basis of the degenerate subspace,

$$|\psi'_\alpha(t)\rangle = \sum_\beta \Omega_{\alpha\beta}(t)|\psi_\beta(t)\rangle. \tag{6.14}$$

From the definition of the vector potential, one readily finds

$$\mathbf{A} \to \mathbf{A}' = i(\nabla_{\boldsymbol{\lambda}}\Omega)\Omega^\dagger + \Omega A \Omega^\dagger, \tag{6.15}$$

i.e., Ω transforms just like a regular nonabelian vector potential. In some cases, this gauge freedom can be used to diagonalize the nonabelian vector potential. In this basis, the path ordering is no longer necessary and the exponent becomes a diagonal matrix whose nonzero entries just take the form of a standard Berry phase.

6.3 Braiding Majorana zero modes

As illustrated in Fig. 6.1, a minimal model for nonabelian braiding starts from a Y-junction of three one-dimensional topological superconductors, labeled wire 1, 2, and 3 [46, 48, 49]. If all three arms are in the topological phase, there are four Majorana bound states in this system. Three of these are located at the outer ends of the three wires, with Bogoliubov operators labeled γ_j for wire j, and a fourth Majorana mode γ_0 is located at the junction of the three wires. As long as the three arms have a finite

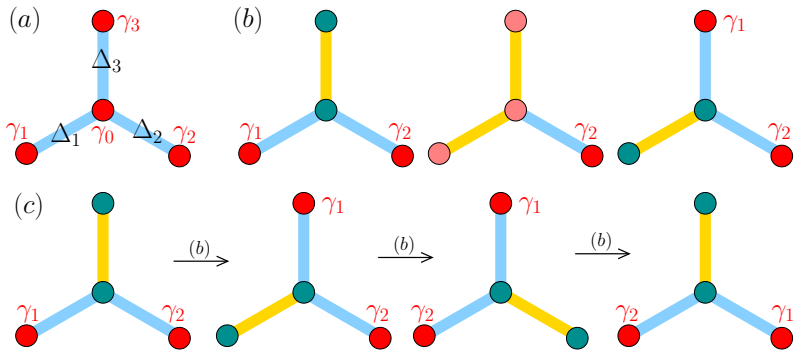

Fig. 6.1 (a) Y-junction with a central Majorana γ_0 and three Majoranas γ_j $(j = 1, 2, 3)$ at the outer ends. The outer Majoranas are coupled to the inner Majorana with strength Δ_j. (b) Basic step of the braiding procedure, which moves a zero-energy Majorana from the end of wire 1 to the end of wire 3 by tuning the Δ_j. Blue (yellow) wires indicate zero (nonzero) couplings Δ_j. Dark red circles correspond to zero-energy Majoranas, green circles indicate Majoranas with finite energy due to coupling. In the intermediate step, the zero-energy Majorana is delocalized over the three pink Majoranas along the yellow wires. (c) Three steps as in (b) braid the zero-energy Majoranas γ_1 and γ_2.

length, these outer Majorana bound states hybridize with the central Majorana and the system is described by the Hamiltonian

$$H = i \sum_{j=1}^{3} \Delta_j \gamma_0 \gamma_j. \tag{6.16}$$

This Hamiltonian couples the central Majorana γ_0 to a linear combination of the outer three Majoranas, $\gamma_\Sigma = (1/E) \sum_{j=1}^{3} \Delta_j \gamma_j$, with proper normalization by $E = [\Delta_1^2 + \Delta_2^2 + \Delta_3^2]^{1/2}$. Thus, the eigenenergies of H are $\pm E$. There are also two linearly independent combinations of the outer Majoranas which do not appear in the Hamiltonian and thus remain true *zero-energy* Majoranas for any (time-independent) choice of the couplings Δ_j. Due to these zero-energy modes, the two eigenvalues of H are each doubly degenerate. These zero-energy Majoranas are particularly simple when just one of the couplings Δ_j is nonzero. In this case, the two zero-energy Majoranas are simply the Majoranas located at the ends of those wires with zero coupling.

The couplings Δ_j can be changed as a function of time. For instance, this can be achieved by varying the length of topological section in each arm: The shorter the topological section, the stronger the overlap and hence the coupling between the outer and the central Majorana. As discussed above, this can be done, say in quantum-wire based realizations, by driving part of the arm into the nontopological phase by the application of a gate voltage or a supercurrent in the adjacent s-wave superconductor. Alternatively, we can leave the length unchanged but vary parameters (such as Zeeman field, induced superconducting pairing correlations, or chemical potential) such that the topological gap of the arm varies. The smaller the topological gap, the larger the spatial extent and hence the overlap of the Majorana end states.

We can now imagine the following braiding procedure [46, 49]. Initially, only Δ_3 in nonzero. Then, γ_1 and γ_2 are zero-energy Majoranas. In a first step, we move a Majorana from the end of wire 1 to the end of wire 3, without involving the zero-energy Majorana γ_2. To this end, first increase Δ_1 to a finite value. The zero-energy Majorana originally located at the end of wire 1 is now delocalized and a linear combination of γ_0, γ_1, and γ_3. We then localize the Majorana zero mode at the end of wire 3 by reducing Δ_3 down to zero, leaving only Δ_1 nonzero. The braiding process is completed by two analogous moves: We first move the zero-energy Majorana from the end of wire 2 to the end of wire 1, and finally the zero-energy Majorana from wire 3 to wire 2. The combined effect of this procedure is to exchange the initial zero-energy Majoranas at the ends of wires 1 and 2.

We will now calculate the adiabatic evolution of the initial state under this braiding protocol. To do so, we introduce conventional fermionic operators through

$$c_1 = \frac{1}{2}(\gamma_1 - i\gamma_2) \quad c_2 = \frac{1}{2}(\gamma_0 - i\gamma_3) \tag{6.17}$$

Using the inverse relations

$$\gamma_1 = c_1 + c_1^\dagger \ ; \ \gamma_2 = i(c_1 - c_1^\dagger) \ ; \ \gamma_3 = i(c_2 - c_2^\dagger) \ ; \ \gamma_0 = c_2 + c_2^\dagger, \tag{6.18}$$

we can write H in terms of c_1 and c_2. We can now write the Hamiltonian in the basis $\{|00\rangle, |11\rangle, |10\rangle, |01\rangle\}$, where the basis states are defined as

$$|11\rangle = c_1^\dagger c_2^\dagger |00\rangle \ , \ |10\rangle = c_1^\dagger |00\rangle \ , \ |01\rangle = c_2^\dagger |00\rangle \tag{6.19}$$

with $c_1|00\rangle = c_2|00\rangle = 0$. This yields

$$H = \begin{pmatrix} \Delta_3 & i\Delta_1 - \Delta_2 & 0 & 0 \\ -i\Delta_1 - \Delta_2 & -\Delta_3 & 0 & 0 \\ 0 & 0 & \Delta_3 & -i\Delta_1 - \Delta_2 \\ 0 & 0 & i\Delta_1 - \Delta_2 & -\Delta_3 \end{pmatrix} \tag{6.20}$$

The block-diagonal structure is a consequence of fermion-number-parity conservation. In fact, it is easy to show that the Hamiltonian H commutes with the fermion-number-parity operator

$$P = \gamma_0\gamma_1\gamma_2\gamma_3. \tag{6.21}$$

The top-left block $H_{\text{even}} = \Delta_3\tau_z - \Delta_1\tau_y - \Delta_2\tau_x$ corresponds to even fermion parity, while the bottom-right block $H_{\text{odd}} = \Delta_3\tau_z + \Delta_1\tau_y - \Delta_2\tau_x$ has odd fermion parity. Here we have defined Pauli matrices τ_i within the even and odd subspaces. If we also define Pauli matrices π_j in the even-odd subspace, then we can write

$$H = \Delta_3\tau_z - \Delta_1\tau_y\pi_z - \Delta_2\tau_x \tag{6.22}$$

for the overall Hamiltonian H. Writing H_{even} and H_{odd} in terms of Pauli matrices makes it obvious that these Hamiltonians take the form of a spin Hamiltonian in magnetic fields $B_{\text{even}} = (-\Delta_2, -\Delta_1, \Delta_3)$ and $B_{\text{odd}} = (-\Delta_2, \Delta_1, \Delta_3)$, respectively. The

degeneracy due to the presence of the Majorana modes implies that the two subspaces have the same eigenvalues. At the same time, the spectrum for each subspace by itself is non-degenerate.

Thus, in the present basis, the nonabelian vector potential is diagonal and in line with Eq. (6.12) its diagonal entries can be computed just as conventional Berry phases. For a spin in a magnetic field, we know that Berry 's phase is just half the solid angle subtended by the unit vector along the magnetic-field direction during the closed trajectory, with opposite signs for the spin-up and the spin-down state [50]. Thus, we can now read off the nonabelian Berry phases for the braiding procedure described above. Let us start with the odd subspace. Then the analog of the Zeeman field is the vector $(-\Delta_2, \Delta_1, \Delta_3)$. The Berry phase is independent of the basis in spin space, and thus we temporarily rotate the basis in $\boldsymbol{\tau}$-space by $-\pi/2$ around the z-axis, so that $\tau_x \to -\tau_y$, $\tau_y \to \tau_x$, and $\tau_z \to \tau_z$. In this rotated basis, the effective magnetic field becomes $\boldsymbol{\Delta} = (\Delta_1, \Delta_2, \Delta_3)$. At the beginning of the braiding process, this field points along the positive z-direction. We first increase Δ_1 and subsequently reduce Δ_3 to zero. Thus, we rotate the unit vector $\boldsymbol{\Delta}$ in the xz-plane to the equator. Next, we increase Δ_2 and reduce Δ_1 to zero. This rotates $\boldsymbol{\Delta}$ by $\pi/2$ around the equator. Finally, we increase Δ_3 and reduce Δ_2 to zero which rotates $\boldsymbol{\Delta}$ back towards the pole. In total, this procedure encloses one quarter of the upper hemisphere, i.e., a solid angle of $\pi/2$, yielding a Berry phase of $\pi/4$, with opposite signs for the spin-up and spin-down states.

To obtain the corresponding phase in the even subspace, we note that the effective Zeeman field in this subspace merely differs in the sign of the y-component. In effect, this implies that the corresponding $\boldsymbol{\Delta}$ encloses the same solid angle but encircles it in the opposite direction. Hence, the Berry phases for the even and odd subspaces are equal in magnitude, but opposite in sign, and we find from Eq. (6.12)

$$U_{12} = e^{i\frac{\pi}{4}\tau_z\pi_z} \tag{6.23}$$

for the exchange of Majoranas 1 and 2. Here, we have dropped the dynamic phase which is the same for all relevant states. Finally, we can reexpress this in terms of the original Majorana operators using the identity $i\gamma_1\gamma_2 = \tau_z\pi_z$ which yields the basis-independent representation

$$U_{12} = e^{i\pi\gamma_1\gamma_2/4} \tag{6.24}$$

of the effect of braiding Majoranas γ_1 and γ_2.

We can check explicitly that the Majorana braiding matrices (6.24) satisfy the defining relations

$$\sigma_i\sigma_j = \sigma_j\sigma_i \qquad |i-j| \leq 2 \tag{6.25}$$

$$\sigma_i\sigma_{i+1}\sigma_i = \sigma_{i+1}\sigma_i\sigma_{i+1} \qquad i = 1\ldots N-1 \tag{6.26}$$

of the braid group. Here, we imagine an N particle system, with the particles ordered and enumerated in some arbitrary fashion as $1, 2, \ldots, N$. Then, σ_i denotes one of $N-1$ generators of the braid group, describing a counterclockwise exchange of particles i and $i+1$. Thus, we can identify σ_i with $U_{i,i+1}$. It is also not difficult to show

that the Majorana braiding matrices (6.24) are indeed nonabelian by showing that $\sigma_i \sigma_{i+1} \neq \sigma_{i+1} \sigma_i$.

7
Experimental signatures

There have been many proposals how to detect Majorana bound states experimentally. In this section, we briefly introduce signatures that have been used in experiment.

7.1 Conductance signatures

7.1.1 Normal-metal lead

A simple and direct method of detecting bound states in superconductors relies on measurements of the tunneling conductance. The differential conductance is nonzero whenever a state in the sample is energetically aligned with the Fermi level in the normal-metal lead. Tuning the bias voltage between lead and sample effectively shifts the Fermi level in the lead and enables measurements as a function of energy. While tunneling into a superconductor is typically suppressed at subgap energies, subgap bound states appear as sharp resonances in the differential conductance.

To understand the nature of transport through such bound states, consider an isolated subgap state that gives rise to a sharp singularity in the density of states. A single electron may tunnel from the lead and occupy the quasiparticle bound state. In the absence of coupling to other degrees of freedom, the quasiparticle cannot relax into the superconductor, thus blocking single-particle transport. In contrast, current can flow by Andreev reflection, when an electron entering from the lead is reflected as a hole, creating a Cooper pair in the sample.

Now, consider a proximity-coupled wire in a topological phase, terminated at one end by a tunnel barrier and connected to a normal-state lead. We calculate the Andreev current from the normal-state lead to the proximity-providing superconductor by scattering theory. The amplitude for an electron in the lead to tunnel through the tunnel barrier, Andreev reflect from the superconductor as a hole, and the hole to tunnel back into the lead is $t_h r_{he} t_e$, where r_{he} (and r_{eh}) are amplitudes for Andreev reflections and t_e (t_h) is the barrier transmission amplitude for electrons (holes). Note that we leave the energy dependence of these amplitudes implicit. In addition, the total current also comprises processes in which the Andreev reflection is followed by a reflection at the barrier and further Andreev reflections. The total amplitude for Andreev reflection is the sum of all of these processes, cf. Fig. 7.1(a),

$$A_{he} = t_h[1 + r_{he}r_e r_{eh} r_h + (r_{he}r_e r_{eh} r_h)^2 + \ldots] r_{he} t_e = \frac{t_h r_{he} t_e}{1 - r_{he} r_e r_{eh} r_h}. \tag{7.1}$$

To obtain the tunneling current, we multiply the Andreev reflection probability $|A_{he}|^2$ by the Fermi distribution of incoming electrons and outgoing holes $n_F(\omega - eV)[1 -$

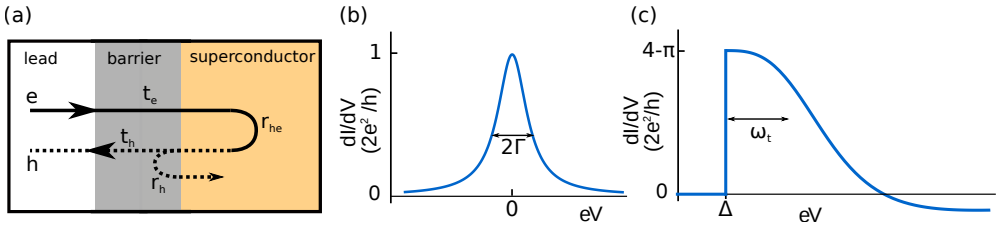

Fig. 7.1 (a) (b) (c)

$n_F(\omega + eV)]$ and integrate over all energies. Note that the electron and hole reservoirs in the lead are shifted relative to the Fermi energy of the sample by $\mp eV$. We further add the contribution due to Andreev reflections of incoming holes and divide by two to prevent double counting. This yields the Andreev current

$$I = \frac{1}{2}\, 2e \int \frac{d\omega}{2\pi\hbar} |A_{he}|^2 [n_F(\omega - eV) - n_F(\omega + eV)] \tag{7.2}$$

for a spinless superconductor, where the charge $2e$ accounts for the fact that a Cooper pair is transmitted during each Andreev reflection.

At subgap energies, the transmission through the superconductor vanishes and the reflection matrix

$$r = \begin{pmatrix} r_{ee} & r_{eh} \\ r_{he} & r_{hh} \end{pmatrix} \tag{7.3}$$

must be unitary. Particle-hole symmetry relates the matrix elements through

$$\tau_x r(-E)\tau_x = r^*(E). \tag{7.4}$$

Specifically, we find $r_{ee} = r_{hh}^*$ and $r_{eh} = r_{he}^*$ at the Fermi energy. This implies that $\det r(E = 0)$ is real. When combined with unitarity, this demands that the determinant of the reflection matrix take on only two possible values,

$$\det r = \pm 1. \tag{7.5}$$

This corresponds to the following two cases, making $\det r$ a topological index: (i) Reflection from the trivial phase with perfect normal reflection $|r_{ee}| = 1$ and zero Andreev reflection $r_{eh} = 0$, corresponding to $\det r = 1$, and (ii) reflection from the topological phase with perfect Andreev reflection $|r_{eh}| = 1$ and zero normal reflection $r_{ee} = 0$. Note that it is impossible to smoothly tune between the two cases.

Before returning to the conductance signatures, we briefly note that this result allows for an alternative derivation of the existence of Majorana bound states. In the topological phase, we find $r_{he} r_{eh} = 1$ at the Fermi level. Consider a topological superconductor terminated by a short normal section and a hard wall. An electron at the Fermi energy impinging on the superconductor is Andreev reflected as a hole, the hole undergoes normal reflection at the hard wall (with phase π) and Andreev reflection from the superconductor, and finally the electron is normally reflected from the hard wall, closing the trajectory. At the Fermi energy, the reflection phases add

to a multiple of 2π, implying the formation of a bound state by Bohr-Sommerfeld quantization. This zero-energy bound state is just the Majorana.

To obtain A_{he} also at nonzero energies, we first recall the Andreev-reflection amplitudes $r_{he} = r_{eh} = \exp[-i \arccos(\omega/\Delta)]$ for an s-wave superconductor with real order parameter $\Delta > 0$. In a p-wave superconductor [see Eq. (2.2)], incoming electron and outgoing hole (both with momentum p_F) experience an effective gap $\Delta = \Delta' p_F$ and thus

$$r_{he} = \exp[-i \arccos(\omega/\Delta)] \tag{7.6}$$

as for the s-wave superconductor. The gap has the opposite sign for the reverse process, as both incoming hole and reflected electron have momentum $-p_F$. The Andreev reflection amplitude is thus

$$r_{eh} = \exp[-i \arccos(\omega/\Delta) + i\pi] = \exp[i \arccos(-\omega/\Delta)] \tag{7.7}$$

In the vicinity of the Fermi level, we can expand

$$r_{he} r_{eh} \simeq 1 + 2i\frac{\omega}{\Delta}, \tag{7.8}$$

and at weak tunneling through the barrier, we can approximate $r_{e/h} \simeq 1 - t_{e/h}^2/2$ (assuming real $r_{e/h}$ and $t_{e/h}$). Using these approximations, we arrive at the Breit-Wigner form

$$|A_{he}|^2 = \frac{t_h^2 t_e^2}{4\omega^2/\Delta^2 + (t_e^2 + t_h^2)^2/4} \tag{7.9}$$

for the Andreev reflection amplitude, and the Andreev current becomes

$$I = e \int \frac{d\omega}{2\pi\hbar} \frac{\Gamma_e \Gamma_h}{\omega^2 + (\Gamma_e + \Gamma_h)^2/4} [n_F(\omega - eV) - n_F(\omega + eV)], \tag{7.10}$$

where we introduced the electron and hole tunneling rates $\Gamma_{e/h} = \frac{1}{2}\Delta t_{e/h}^2$ through the barrier. These can be evaluated at the Fermi level, where they are equal by particle-hole symmetry, $\Gamma_e = \Gamma_h = \Gamma$. The resonance of the integrand (7.10) at energy $\omega = 0$ reflects the Majorana bound state at the junction.

Using Eq. (7.10) to compute the differential conductance, we find

$$\frac{\mathrm{d}I}{\mathrm{d}V} = \frac{2e^2}{h} \frac{\Gamma^2}{eV^2 + \Gamma^2}. \tag{7.11}$$

The differential conductance is a Lorentzian as a function of bias voltage, with quantized height $2e^2/h$ and peak width determined by the tunneling rate through the barrier, see Fig. 7.1(b) [53, 54]. This quantized zero-bias conductance peak can serve as a robust fingerprint of an isolated Majorana bound state. For other subgap states such as regular Andreev bound states, the conductance is not restricted to quantized values. Moreover, such resonances will typically shift in energy as function of gate voltage or magnetic field.

Nevertheless, it remains a challenging task to resolve this quantized conductance peak in experiment. First, temperature broadening of the distribution function in

the normal lead limits the energy resolution. Once temperature exceeds the intrinsic broadening Γ, the width of the conductance peak is determined by temperature T, and the conductance peak is correspondingly reduced by a factor of order Γ/T. The situation may be particularly unfavorable in multichannel wires, where the coupling of the topological channel to the lead is typically very weak [52].

Second, the zero-bias Majorana peak is also broadened by inelastic quasiparticle transitions in the superconductor. At finite temperatures, there will be inelastic (e.g., phonon-assisted) transitions of quasiparticles between the zero-energy state and other subgap states or the quasiparticle continuum. These quasiparticle-poisoning processes reduce the lifetime of the zero-energy excitation and can be accounted for phenomenologically in Eq. (7.11) by including an additional rate Γ_{qp} into the broadening,

$$\frac{dI}{dV} = \frac{2e^2}{h} \frac{\Gamma^2}{eV^2 + (\Gamma + \Gamma_{qp})^2}. \tag{7.12}$$

Thus quasiparticle poisoning also destroys the conductance quantization at zero bias. In addition, such relaxation processes of quasiparticles allow for an additional single-particle current which is nonquantized and adds to the Andreev current [55, 56].

7.1.2 Superconducting lead

An alternative experiment tunnels into the Majorana bound state from a (nontopological) superconducting tip. One advantage of this setup is that the gap exponentially suppresses finite-temperature broadening. It is important to understand that for a superconducting electrode, Majorana bound states are no longer signaled by zero-bias peaks. The threshold for electron tunneling corresponds to the Majorana bound state overlapping with the BCS singularity in the density of states of the electrode. Thus, the Majorana bound state is signaled by differential conductance peaks at bias voltages $eV = \pm\Delta$, where Δ denotes the gap of the electrode.

Heuristically, we can derive the tunneling current from Eq. (7.10) by noting that the tunneling rates Γ_e and Γ_h are proportional to the density of states in the lead electrode. In a superconductor, we thus expect $\Gamma_{e/h} = \Gamma\rho(\omega \mp eV)$ with the dimensionless BCS density of states $\rho(\omega) = \theta(|\omega| - \Delta)|\omega|/\sqrt{\omega^2 - \Delta^2}$ normalized to the normal-state density of states. It can indeed be shown that this is the result of a more formal calculation, see [57].

Up to exponentially small corrections in $\Delta/T \gg 1$ and for $eV \simeq \Delta$, we can set $n_F(\omega - eV) - n_F(\omega + eV) \simeq 1$ (refelcting the above-mentioned insensivity to temperature). Then, the current becomes

$$I = e \int_{-(eV-\Delta)}^{eV-\Delta} \frac{d\omega}{2\pi\hbar} \frac{\Gamma^2 \rho(\omega - eV)\rho(\omega + eV)}{\omega^2 + \Gamma^2[\rho(\omega - eV) + \rho(\omega + eV)]^2/4}. \tag{7.13}$$

In this low-temperature limit, the current vanishes for $eV < \Delta$. We measure voltage from the threshold, $\eta = eV - \Delta$, so that for $\eta \simeq 0$ the bound state is energetically aligned with the BCS singularities of the lead. For $|\omega| < \eta$ we can approximate

$$\rho(\omega \pm eV) \simeq \sqrt{\Delta/2(\eta \pm \omega)} \gg 1. \tag{7.14}$$

This yields the current

$$I = \frac{4e}{h} \int_{-\eta}^{\eta} \frac{d\omega}{\sqrt{\eta^2 - \omega^2}} \frac{\omega_t^3}{\omega^2 + \omega_t^3 \left(\frac{1}{\sqrt{\eta - \omega}} + \frac{1}{\sqrt{\eta + \omega}} \right)^2}, \tag{7.15}$$

where we introduced the effective tunnel coupling $\omega_t = (\Delta\Gamma^2)^{1/3}/2$. We finally arrive at

$$I = \frac{4e}{h} \eta \int_{-1}^{1} \frac{dx}{\sqrt{1 - x^2}} \frac{1}{x^2 (\eta/\omega_t)^3 + \left(\frac{1}{\sqrt{1-x}} + \frac{1}{\sqrt{1+x}} \right)^2} \tag{7.16}$$

for $\eta > 0$, with the limiting cases

$$\frac{dI}{dV} = \begin{cases} 0 & eV - \Delta < 0 \\ \frac{2e^2}{h}(4 - \pi) & eV - \Delta = 0 \\ -\frac{2e^2}{h} \frac{\omega_t^3}{(eV - \Delta)^3} \times \text{const.} & eV - \Delta \gg \omega_t \end{cases}. \tag{7.17}$$

The conductance is shown in Fig. 7.1(c). At $eV = \Delta$, the conductance jumps from zero to the maximal value $(4 - \pi)\frac{2e^2}{h}$ and then decreases on the scale ω_t, eventually developing a shallow negative differential conductance dip.

This result has several remarkable implications [57]: (a) The peak conductance is universal, independent of tunneling strength, Majorana wavefunction, or the sign of the voltage. This parallels the conductance quantization for a normal-metal tip. For both normal-state and superconducting electrodes, conventional subgap states exhibit nonuniversal behavior, so that they can in principle be distinguished from Majorana resonances. (b) The peak width depends on a lower power of the tunneling strength for a superconducting electrode, $\sim \Gamma^{2/3}$, than for a normal-state electrode, $\sim \Gamma$. This weak dependence on the junction transmission allows one to distinguish bound state resonances from competing multiple Andreev peaks whose width scales as Γ^2. (c) Thermal broadening is practically irrelevant for a superconducting lead at $T \ll \Delta$. (d) For a superconducting lead, the peak conductance is less vulnerable to quasiparticle poisoning. At the threshold $eV = \Delta$, the tunneling rates $\Gamma_{e/h}$ diverge due to the BCS singularity, making additional broadening due to inelastic transitions ineffective.

This leads to a striking Majorana signature when using a superconducting scanning tunneling microscope tip and mapping out the conductance in the vicinity of the bound state. For a Majorana state, the threshold conductance is independent of the location of the tip, and the Majorana appears as a plateau of height $(4 - \pi)(2e^2/h)$. The extension of the plateau is only limited by experimental resolution.

7.2 4π-periodic Josephson effect

So far, we considered junctions of a topological superconductor with a normal metal or a conventional superconductor. Junctions of two topological superconductors, harboring two Majorana bound states γ_L and γ_R, provide additional signatures. The coupling across the junction fuses the two Majoranas into a conventional fermion with nonzero energy. Nevertheless, the junction retains important signatures of the topological phase in the two superconductors.

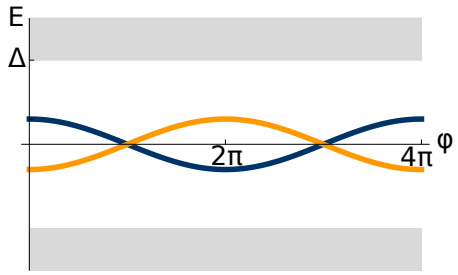

Fig. 7.2 Subgap

This is rooted in the bound state spectrum of the junction, which can be obtained from the tunneling Hamiltonian

$$H_T = tc_L^\dagger c_R + t^* c_R^\dagger c_L, \tag{7.18}$$

which couples the topological superconductors. Here, t is the tunneling matrix element and the operator $c_{L/R}$ annihilates an electron at the junction in the left/right superconductor. When the two banks of the junction have the same superconducting phase, the projection of the tunneling Hamiltonian onto the low-energy Majorana excitations reads

$$H_T = (t + t^*) u_L u_R P, \tag{7.19}$$

where $P = i\gamma_L\gamma_R$ is the parity operator of the fermion formed of the two Majoranas. Here, we used that the electron operators project as $c_L \simeq u_L\gamma_L$ and $c_R \simeq iu_R\gamma_R$, where $u_{L/R}$ are real Majorana wavefunctions in the left and right bank. Indeed, these expressions are consistent with the results for the Kitaev chain in Sec. 5.3 for $t = \Delta$ and $\mu = 0$, where the low-energy projections of the two end fermions are $c_1 \simeq i\gamma_{A1}$ and $c_N \simeq \gamma_{BN}$.

In an appropriate gauge, a phase difference φ across the junction can be incorporated entirely into the tunneling amplitude, $t = t_0 e^{i\varphi/2}$ with t_0 real. Thus, we find the phase-dependent subgap spectrum

$$E = \pm 2\cos(\varphi/2) t_0 u_L u_R, \tag{7.20}$$

where the sign corresponds to the parity eigenvalue ± 1. This is illustrated in Fig. 7.2. Remarkably, E is 4π-periodic for fixed parity and tuning the phase by 2π changes the energy of the system! Of course, the entire spectrum, including both fermion parity sectors, is 2π-periodic as required by gauge invariance.

For fixed fermion parity, this result predicts a 4π-periodic Josephson current, quite unlike the 2π-periodic Josephson current of conventional Josephson junctions. This remarkable consequence of Majorana physics follows when recalling that the Josephson current can be obtained from the subgap spectrum through

$$I = 2e\frac{dE}{d\varphi}, \tag{7.21}$$

as can be readily established from the tunneling Hamiltonian (7.18) with $t = t_0 e^{i\varphi/2}$. For fixed fermion parity, only one of the subgap states contributes and the Josephson current has period 4π. We also observe that the Josephson current has the same magnitude, but opposite signs for the two fermion parities.

An important point of this argument is that there is a degeneracy of the two states at $\varphi = \pi$. The Josephson behavior would revert to the conventional 2π periodicity, should this crossing turn into an anticrossing. However, this cannot happen as the crossing is protected by fermion parity! The crossing of the subgap states at $\varphi = \pi$ implies a ground-state degeneracy and can be viewed as a quantum phase transition, at which the fermion parity of the many-body ground state changes.

It is also interesting to connect these considerations with our discussion of symmetry classes in Sec. 2.1. For $\varphi = \pi$, the pairing gaps have opposite sign in the two banks. As discussed in Sec. 2.1, each bank is described by a Hamiltonian in class BDI, albeit with opposite topological indices ± 1. Hence, the topological index jumps by 2 across the junction, which necessitates the presence of two Majorana bound states, in agreement with our findings. The protection of these two Majoranas relies on chiral symmetry, which is broken by the complex order parameter away from $\varphi = \pi$ and hence the energy levels split.

Experimental observation of the 4π-periodic Josephson effect requires that fermion parity is preserved. If the phase difference is varied too slowly, parity may change by quasiparticle poisoning, masking the 4π periodicity. One way of varying the phase difference swiftly is via the *ac* Josephson effect in the presence of a finite bias voltage across the junction. The 4π periodicity generates an *ac* current at half the usual Josephson frequency, a clear signature of topological superconductivity. However, one needs to keep in mind that the time-dependent phase difference may induce diabatic transitions between the low-energy bound states and the quasiparticle continuum above the gap. Such transitions are most likely in the vicinity of the phase difference where the bound-state energy becomes maximal, and cause switching between the fermion parities. This also masks the fractional Josephson frequency. Even in the presence of these transitions, however, a signature remains present in the finite-frequency current noise, which has a peak at half the Josephson frequency [58]. This effect is particularly prominent at low bias voltages when transitions occur only after many cycles.

An alternative route, which requires only static measurements, is based on Shapiro steps. In conventional junctions, the combination of a *dc* voltage V_{dc} and an ac voltage $V_{ac}\sin(\omega t)$ generates a Josephson current

$$I = I_J \sin(\varphi + 2eV_{dc}t - (eV_{ac}/\omega)\cos(\omega t)). \tag{7.22}$$

Expanding this expression in Bessel functions, one can show that the current exhibits steps as a function of bias voltage. These steps originate from resonances between the *ac* voltage and the phase winding due to the *dc* voltage, which occur when $2eV_{dc} = n\omega$ with n an integer. Clearly, this condition is modified when the current-phase relation is 4π-periodic and the steps occur instead at $eV_{dc} = n\omega$. Thus, Majoranas only contribute to every second Shapiro step, predicting a prominent even-odd asymmetry of the Shapiro steps as a strong signatures of Majorana states.

8
Conclusions

In these notes, we have provided an introduction into the physics of one-dimensional topological superconductivity and Majorana bound states. This field is currently attracting significant theoretical and experimental attention. It is fueled by the prospect of not only establishing the existence of these exotic quasiparticles, but of observing a new type of quantum statistics. Condensed matter has already enriched physics through the (abelian) anyonic statistics of the quasiparticles in the fractional quantum Hall effect. Observing nonabelian statistics would take this to yet another level. It is quite remarkable that such fundamentally new physics is lurking in material systems as mundane as hybrids of semiconductors and superconductors, with the relevant phases accessible to a standard mean-field analysis. This contrasts sharply with the abelian anyons which occur in the strongly correlated fractional quantum Hall states.

Beyond the nonabelian statistics, the field is energized by its potential for topological quantum information processing. One envisions to exploit the remarkable properties of Majorana bound states to store and process quantum information in an intrinsically fault-tolerant manner. However, it turns out that it is impossible to construct a universal topological quantum computer based on braiding Majorana bound states. Two possible workarounds are being discussed in the literature: The less ambitious but perhaps more realistic approach is to complement the topologically protected braiding operations by additional gate operations which are unprotected. In addition to the topologically protected gate operations based on Majorana braiding, it would suffice to include the unprotected operation $\exp(i\pi\gamma_j\gamma_{j+1}/8)$. Even when including such nontopological gate operations, one would still gain significantly from the topological protection of information storage and the partial protection of information processing. The more ambitious program tries to find platforms which realize yet more exotic quasiparticles such as Fibonacci anyons with a richer braid group and the capacity to realize a universal topological quantum computer.

There are many aspects of Majorana physics which are not discussed in these notes, such as effects of disorder and interactions, alternative experimental platforms, as well as numerous proposals for experimental Majorana signatures. Most importantly, we did not discuss the existing experiments in any detail. However, we hope that these notes provide sufficient detail for readers to develop their own informed opinion on these and forthcoming experiments.

Acknowledgements

We would like to acknowledge our collaborators on this subject from whom we learned much of what we know. These are Jason Alicea, Erez Berg, Arne Brataas, Piet Brouwer, Matthias Duckheim, Matthew Fisher, Katharina Franke, Leonid Glazman, Arbel Haim, Bert Halperin, Benjamin Heinrich, Liang Jiang, Torsten Karzig, Graham Kells, Yuval Oreg, David Pekker, Armin Rahmani, Gil Refael, Alessandro Romito, Michael Ruby, Ady Stern, and Yuval Vinkler. We would also like to acknowledge financial support through the Helmholtz Virtual Institute "New States of Matter and Their Excitations" as well as the DFG Priority Program "Topological Insulators."

Appendix A
Pairing Hamiltonians: BdG and 2nd quantization

Up to a constant, a general second-quantized pairing Hamiltonian $\mathcal{H}$ can be brought into Bogoliubov-de Gennes form by doubling the degrees of freedom,

$$\mathcal{H} = \frac{1}{2}\int d^d x \Psi^\dagger(x) H \Psi(x) + const. \tag{A.1}$$

where H is the first-quantized Bogoliubov-de Gennes (BdG) Hamiltonian. Throughout these notes, we choose the Nambu spinor ordered as

$$\Psi(x) = (\psi_\uparrow(x), \psi_\downarrow(x), \psi_\downarrow^\dagger(x), -\psi_\uparrow^\dagger(x))^T. \tag{A.2}$$

As an example, consider the second-quantized Hamiltonian for the topological insulator edge,

$$\begin{aligned}\mathcal{H} = \int dx \Big\{ & -iv_F \left[\psi_\uparrow^\dagger(x)\partial_x\psi_\downarrow(x) + \psi_\downarrow^\dagger(x)\partial_x\psi_\uparrow(x)\right] \\ & -B\left[\psi_\uparrow^\dagger(x)\psi_\uparrow(x) - \psi_\downarrow^\dagger(x)\psi_\downarrow(x)\right] + \Delta\left(\psi_\uparrow^\dagger(x)\psi_\downarrow^\dagger(x) + h.c\right)\Big\}.\end{aligned} \tag{A.3}$$

Introducing Nambu spinor and using the anticommutation relations of the electronic operators, we can bring this Hamiltonian into the BdG form (A.1) with the BdG Hamiltonian H given by Eq. (3.1).

With the definition (A.2) of the spinor, time reversal is effected by

$$T = i\sigma_y K, \tag{A.4}$$

where K denotes complex conjugation, and charge conjugation by

$$C = -i\tau_y. \tag{A.5}$$

Due to the doubling of the degrees of freedom, the BdG Hamiltonian acquires the constraint

$$CT\Psi = \Psi, \tag{A.6}$$

known as particle-hole symmetry. For the BdG Hamiltonian, particle-hole symmetry implies

$$\{H, CT\} = 0, \quad CT\Psi = \Psi. \tag{A.7}$$

Denote the eigenfunctions of H as $\Phi_n(x) = (u_{\uparrow,n}(x), u_{\downarrow,n}(x), v_{\uparrow,n}(x), v_{\downarrow,n}(x))^T$ with eigenvalues E_n, satisfying

$$H\Phi_n(x) = E_n\Phi_n(x). \tag{A.8}$$

This equation is known as the BdG equation. Particle-hole symmetry implies

$$HCT\Phi_n = -CTH\Phi_n = -CTE_n\Phi_n = -E_nCT\Phi_n, \tag{A.9}$$

for every BdG eigenspinor Φ_n with energy E_n, there is an eigenspinor $\Phi_{-n} = CT\Phi_n$ with energy $-E_n$. The eigenspinors are orthonormal,

$$\int dx\Phi_n^\dagger(x)\Phi_m(x) = \delta_{nm}, \tag{A.10}$$

where δ_{nm} is the Kronecker symbol when $\Phi_n(x)$ and $\Phi_m(x)$ are normalizable and a Dirac δ-function when $\Phi_n(x)$ and $\Phi_m(x)$ are scattering states. In addition, the completeness can be written as

$$\sum_n \Phi_n(x)\Phi_n^\dagger(y) = \delta(x-y). \tag{A.11}$$

Using the BdG eigenspinors, the second-quantized Hamiltonian (A.1) can be written as (up to a constant)

$$\begin{aligned}
\mathcal{H} &= \frac{1}{2}\int dx\Psi^\dagger(x)H\Psi(x) && \text{(A.12)}\\
&= \int dx\int dy\Psi^\dagger(y)H\delta(x-y)\Psi(x) && \text{(A.13)}\\
&= \sum_n \int dxdy\Psi^\dagger(y)H\Phi_n(y)\Phi_n^\dagger(x)\Psi(x) && \text{(A.14)}\\
&= \sum_n E_n\gamma_n^\dagger\gamma_n, && \text{(A.15)}
\end{aligned}$$

where the γ_n are the Bogoliubov quasiparticle operators. They can be expressed in terms of the original electron operators as

$$\begin{aligned}
\gamma_n &= \int dx\Phi_n^\dagger(x)\Psi(x) && \text{(A.16)}\\
\gamma_n^\dagger &= \int dx\Psi^\dagger(x)\Phi_n(x). && \text{(A.17)}
\end{aligned}$$

Using Eq. (A.7), (A.9), and the unitarity CT, we have

$$\begin{aligned}
\gamma_{-n}^\dagger &= \int dx\Psi^\dagger(x)\Phi_{-n}(x)\\
&= \int dx\left[CT\Psi(x)\right]^\dagger\left[CT\Phi_n(x)\right]\\
&= \int dx\,\Phi_n^\dagger(x)\Psi(x) = \gamma_n. && \text{(A.18)}
\end{aligned}$$

One can readily check that the Bogoliubov operators fulfill the fermionic anticommutation relations.

We can also write the electronic operators in terms of Bogoliubov operators by using Eq. (A.11),

$$\begin{aligned}\Psi(x) &= \sum_n \Phi_n(x)\gamma_n = \sum_{n>0} \left(\Phi_n(x)\gamma_n + \Phi_{-n}(x)\gamma_{-n}\right) \\ &= \sum_{n>0} \left(\Phi_n(x)\gamma_n + CT\Phi_n(x)\gamma_n^\dagger\right). \end{aligned} \tag{A.19}$$

These equations have to be complemented by the Majorana mode when there is an isolated zero-energy eigenspinor with associated Bogoliubov operator $\gamma_0 = \gamma_0^\dagger$, see Sec. 3.2.

Appendix B
Proximity-induced pairing

All realizations of topological superconducting phases discussed in these notes are based on proximity-induced superconductivity. At the same time, we never explicitly discussed the s-wave superconductor which induces the superconducting correlations in the one-dimensional system. Instead, we directly included a pairing term in the Bogoliubov-de Gennes Hamiltonian of the one-dimensional system. In this appendix, we want to briefly discuss the proximity effect more explicitly for a one-dimensional wire proximity coupled to a BCS superconductor, not accounting for Zeeman fields or spin-orbit coupling.

The s-wave superconductor is described by the pairing Hamiltonian

$$\mathcal{H}_s = \frac{1}{2}\int d^3r\, \psi^\dagger(\mathbf{r}) H_s \psi(\mathbf{r}) \tag{B.1}$$

$$H_s = \xi_{\mathbf{p}}\tau_z + \Delta\tau_x \tag{B.2}$$

$$\xi_{9\mathbf{p}} = \frac{\mathbf{p}^2}{2m} - \mu, \tag{B.3}$$

written in terms of the Nambu spinor

$$\psi(\mathbf{r}) = \left(\psi_\uparrow(\mathbf{r}), \psi_\downarrow(\mathbf{r}), \psi_\downarrow^\dagger(\mathbf{r}), -\psi_\uparrow^\dagger(\mathbf{r})\right)^T. \tag{B.4}$$

Here, Δ is the s-wave gap of the proximity-providing superconductor, and the τ_i denote Pauli matrices in Nambu space. The one-dimensional wire can is modeled by the Bogoliubov–de Gennes Hamiltonian

$$\mathcal{H}_d = \frac{1}{2}\int dx\, d^\dagger(x) H_d d(x) \tag{B.5}$$

where

$$d(x) = \left(d_\uparrow(x), d_\downarrow(x), d_\downarrow^\dagger(x), -d_\uparrow^\dagger(x)\right)^T. \tag{B.6}$$

At low energies in the vicinity of the Fermi energy, we can the dispersion of the wire, so that its Bogoliubov–de Gennes Hamiltonian becomes

$$H_d = v_F p_x \tau_z, \tag{B.7}$$

with the momentum p_x measured from the respective Fermi point. The hybridization between the adatom chain and the superconductor is modeled by

$$\mathcal{H}_T = -\frac{t}{2}\int d^3r\ \left[\psi^\dagger(\mathbf{r})\tau_z d(x) + d^\dagger(x)\tau_z\psi(\mathbf{r})\right]\delta(y)\delta(z), \tag{B.8}$$

which describes local tunneling between wire and superconductor.

In order to describe the effect of the superconductor on the wire, we consider the Green function of the electrons in the wire and account for the coupling to the superconductor through a self energy. Since we are dealing with a quadratic problem, this self energy can be computed exactly,

$$\Sigma(x_1 - x_2, E) = t^2\tau_z g_s(\mathbf{x}_1 - \mathbf{x}_2, E)\tau_z, \quad \mathbf{x}_i = (x_i, 0, 0), \tag{B.9}$$

where $g_s(\mathbf{r})$ is the real-space Green function of the uncoupled BCS superconductor. We also used the translational invariance of the adatom chain along the x-direction so that the self-energy only depends on the distance between the two positions. The Green function of the superconductor can now be evaluated as

$$g_s(\mathbf{x}_1 - \mathbf{x}_2, E) = \int \frac{d^3p}{(2\pi)^3}\frac{e^{i(x_1-x_2)p_x}}{E - \Delta\tau_x - \xi_p\tau_z} \tag{B.10}$$

$$\simeq \nu_0^{2D}\int\frac{dp_x}{2\pi}e^{i(x_1-x_2)p_x}\int d\xi\frac{E+\Delta\tau_x}{E^2-\Delta^2-\xi^2} \tag{B.11}$$

$$= -\pi\nu_0^{2D}\frac{E+\Delta\tau_x}{\sqrt{\Delta^2-E^2}}\delta(x_1-x_2). \tag{B.12}$$

Here, ν_0^{2D} is a two-dimensional density of states at the Fermi level. Note that to a good approximation, the self energy is strictly local. Thus, it becomes independent of momentum when Fourier transforming to momentum space along the x-direction,

$$\Sigma(k, E) = -\Gamma_{2D}\frac{E - \Delta\tau_x}{\sqrt{\Delta^2 - E^2}}, \quad \Gamma_{2D} = \pi\nu_0^{2D}t^2 \tag{B.13}$$

We thus find the dressed Green function

$$G_s(k, E) = [g_s^{-1}(k, E) - \Sigma(k, E)]^{-1} \tag{B.14}$$

describing the propagation of electrons in the quantum wire.

To understand this self energy better, it is instructive to consider various limits. For $E \gg \Delta$, i.e., for energies far above the gap, we find the retarded self energy

$$\Sigma^R(k, E) \simeq -i\Gamma_{2D} \tag{B.15}$$

The self energy is purely imaginary and describes the fact that high-energy excitations in the wire can decay into the superconductor with rate $2\Gamma_{2D}$. Indeed, the $2\Gamma_{2D} = 2\pi\nu_0^{2D}t^2$ just coincides with a simple golden-rule result for this process at fixed k, as the density of states of the superconductor is unaffected by pairing at high energies.

At subgap energies, $E \ll \Delta$, the self energy is purely real, reflecting the fact that the superconductor is gapped and excitations in the wire can only virtually enter the

superconductor, but not decay into it. We can now expand the self energy for small E,

$$\Sigma(k,E) \simeq -\frac{\Gamma_{2D}}{\Delta}E - \Gamma_{2D}\tau_x. \tag{B.16}$$

At first sight, the induced gap is given by Γ_{2D}. However, this cannot be the case at strong hybridization $\Gamma_{2D} \gg \Delta$. In fact, in this limit, the term linear in E becomes important and induces a significant renormalization of the quasiparticle weight,

$$\begin{aligned} G_s(k,E) &= [E(1+\Gamma_{2D}/\Delta) - v_F k\tau_z - \Gamma_{2D}\tau_x]^{-1} \\ &= \frac{Z}{E - Zv_F k\tau_z + Z\Gamma_{2D}\tau_x}, \end{aligned} \tag{B.17}$$

where

$$Z = \frac{1}{1+\Gamma_{2D}/\Delta}. \tag{B.18}$$

This renormalization of the quasiparticle weight reflects the fact that even at subgap energies, excitations of the quantum wire have appreciable spectral weight in the superconductor. We can now identify the induced gap

$$\Delta_{\text{ind}} = Z\Gamma_{2D} \simeq \begin{cases} \Gamma_{2D} & \Gamma_{2D} \ll \Delta \\ \Delta & \Gamma_{2D} \gg \Delta \end{cases}. \tag{B.19}$$

We observe that as a result of the renormalization of the quasiparticle weight, the induced gap indeed saturates at the host gap as expected.

However, this renormalization also has other important consequences. The dispersion is obtained from the poles of the Green function,

$$\det G_s^{-1}(k,E) = 0 \tag{B.20}$$

for each k. This yields

$$E(k) = \pm\sqrt{(Zv_F k)^2 + (Z\Gamma_{2D})^2}. \tag{B.21}$$

Thus, at strong hybridization, $\Gamma_{2D} \gg \Delta$, there is also a significant renormalization of the Fermi velocity v_F,

$$v_F \to \tilde{v}_F = v_F \frac{\Delta}{\Gamma_{2D}}. \tag{B.22}$$

This implies that also the effective coherence length of the proximity-induced superconducting correlations in the wire can be quite different from the coherence length of the superconductor. If we assume that both wire and superconductor have bare Fermi velocities of the same order (as is presumably the case in the adatom scenario), the correlation length of the proximity-induced superconductivity is

$$\xi = \frac{\hbar\tilde{v}_F}{\Delta_{ind}} = \frac{\hbar v_F}{\Gamma_{2D}}. \tag{B.23}$$

At strong hybridization, this is much smaller than the coherence length of the bulk superconductor, $\hbar v_F/\Delta$.

Appendix C
Shiba states

In this appendix, we outline the derivation of the Shiba states for a single magnetic impurity. We first consider the approach in which the adatom is described as a classical magnetic moment. Subsequently, we describe the adatom as a spin-1/2 Anderson impurity, treating the onsite interaction within a mean-field approximation.

C.1 Adatom as a classical magnetic impurity

Our starting point is the Hamiltonian in Eq. (5.1). When choosing the impurity spin $\mathbf{S}$ to point along the z direction, this 4×4 Hamiltonian separates into independent 2×2 blocks $\mathcal{H}_\pm$ for spin-up $(+)$ and spin-down $(-)$ electrons,

$$\mathcal{H}_\pm = \xi_{\mathbf{p}} \tau_z [V \tau_z \mp JS] \delta(\mathbf{r}) + \Delta \tau_x. \tag{C.1}$$

To solve for the bound-state spectrum, we isolate the impurity terms on the right-hand side,

$$[E - \xi_{\mathbf{p}} \tau_z - \Delta \tau_x] \psi(\mathbf{r}) = [V \tau_z \mp JS] \delta(\mathbf{r}) \psi(\mathbf{0}), \tag{C.2}$$

and pass to momentum representation, $\psi(\mathbf{r}) = \int [d\mathbf{p}/(2\pi)^3] \psi_{\mathbf{p}}$. This yields

$$[E - \xi_{\mathbf{p}} \tau_z - \Delta \tau_x] \psi_{\mathbf{p}} = [V \tau_z \mp JS] \psi(\mathbf{0}). \tag{C.3}$$

and hence

$$\psi_{\mathbf{p}} = \frac{1}{E - \xi_{\mathbf{p}} \tau_z - \Delta \tau_x} [V \tau_z \mp JS] \psi(\mathbf{0}). \tag{C.4}$$

We can now obtain an equation for the spinor $\psi(\mathbf{0})$ evaluated at the position of the impurity only,

$$\psi(\mathbf{0}) = \int \frac{d\mathbf{p}}{(2\pi)^3} \frac{E + \xi_{\mathbf{p}} \tau_z + \Delta \tau_x}{E^2 - \xi_{\mathbf{p}}^2 - \Delta^2} [V \tau_z \mp JS] \psi(\mathbf{0}). \tag{C.5}$$

For subgap energies $E < \Delta$, the integral can be readily performed. This yields

$$\left\{ \mathbf{1} + \frac{E + \Delta \tau_x}{\sqrt{\Delta^2 - E^2}} [\beta \tau_z \mp \alpha] \right\} \psi(\mathbf{0}) = 0. \tag{C.6}$$

Here we introduced the dimensionless measures $\alpha = \pi \nu_0 JS$ and $\beta = \pi \nu_0 V$ of the exchange coupling and the potential scattering, respectively. ν_0 denotes the normal-phase density of states.

Setting the determinant of the prefactor of $\psi(\mathbf{0})$ in Eq. (C.6) equal to zero, we find that $\mathcal{H}_\pm$ has a subgap solution with energies

$$E = \pm\Delta \frac{1-\alpha^2+\beta^2}{\sqrt{(1-\alpha^2+\beta^2)^2+4\alpha^2}}. \tag{C.7}$$

The positive (negative) sign corresponds to the spin-up (spin-down) sector. The energies of the two Shiba states cross at zero when $\alpha^2 = 1+\beta^2$. For stronger exchange coupling, the ground state changes from even to odd electron number. Notice also that $E_0 \to \Delta$ for vanishing exchange coupling, $\alpha \to 0$, in accordance with Anderson's theorem.

Inserting these eigenenergies into Eq. (C.6), we can obtain the corresponding eigenspinors,

$$\psi(\mathbf{0}) = \begin{pmatrix} u(\mathbf{0}) \\ v(\mathbf{0}) \end{pmatrix} = C \begin{pmatrix} \sqrt{1+(\alpha\pm\beta)^2} \\ \pm\sqrt{1+(\alpha\mp\beta)^2} \end{pmatrix} \tag{C.8}$$

where C is a normalization constant. The normalization constant can be found from the condition

$$\int \frac{d\mathbf{p}}{(2\pi)^3}(|u_\mathbf{p}|^2 + |v_\mathbf{p}|^2) = 1, \tag{C.9}$$

where

$$\psi_\mathbf{p} = \begin{pmatrix} u_\mathbf{p} \\ v_\mathbf{p} \end{pmatrix} \tag{C.10}$$

is given in Eq. (C.4). A somewhat length, but elementary evaluation of this condition yields

$$\psi_\mathbf{p} = \frac{\sqrt{2\pi\alpha\nu_0\Delta}}{[(1+(\alpha-\beta)^2)(1+(\alpha+\beta)^2)]^{3/4}} \begin{pmatrix} \sqrt{1+(\alpha\pm\beta)^2} \\ \pm\sqrt{1+(\alpha\mp\beta)^2} \end{pmatrix}. \tag{C.11}$$

It is interesting to make two comment:

- Even when $E = 0$, i.e., for $\alpha^2 - \beta^2 = 1$, the electron and hole wavefunctions of the Shiba state are in general different from one another. This is quite distinct from Majorana zero-energy states for which electron and hole wavefunctions are necessarily complex conjugates of one another.
- Electron and hole wavefunctions do become equal up to a sign in the absence of potential scattering.

Finally, we can also give the four-spinor results for the Shiba state wavefunctions at the position of the impurity,

$$\psi_+(\mathbf{0}) = \frac{\sqrt{2\pi\alpha\nu_0\Delta}}{[(1+(\alpha-\beta)^2)(1+(\alpha+\beta)^2)]^{3/4}} \begin{pmatrix} \sqrt{1+(\alpha+\beta)^2} \\ 0 \\ \sqrt{1+(\alpha-\beta)^2} \\ 0 \end{pmatrix} \tag{C.12}$$

$$\psi_-(\mathbf{0}) = \frac{\sqrt{2\pi\alpha\nu_0\Delta}}{[(1+(\alpha-\beta)^2)(1+(\alpha+\beta)^2)]^{3/4}} \begin{pmatrix} 0 \\ \sqrt{1+(\alpha-\beta)^2} \\ 0 \\ -\sqrt{1+(\alpha+\beta)^2} \end{pmatrix}. \quad \text{(C.13)}$$

C.2 Adatom as a spin-1/2 Anderson impurity

Following the main text, we focus on the case when the impurity level is fully spin polarized along z-axis so that $\langle n\rangle = 1$ and $\langle m\rangle = 1$. Using the Nambu spinor notation

$$d = \left(d_\uparrow, d_\downarrow, d_\downarrow^\dagger, -d_\uparrow^\dagger\right)^T, \quad \text{(C.14)}$$

we can write down the Bogoliubov-de Gennes Hamiltonian for the impurity level as

$$\begin{aligned} \mathcal{H}_d &= \frac{1}{2} d^\dagger H_d d \\ H_d &= (\epsilon_d - \mu + \frac{U}{2})\tau_z + \frac{U}{2}\sigma_z. \end{aligned} \quad \text{(C.15)}$$

The adatom induces localized subgap states once the the hybridization with the superconductor is included. The spectrum of subgap states can be found from the poles of the local Green function $G(E)$ of the superconductor at the impurity position (chosen at the origin). Due to the local nature of the tunneling, the latter obeys a purely multiplicative Dyson equation

$$G(E) = g(E) + g(E)\Sigma(E)G(E) \quad \text{(C.16)}$$

where $g(E)$ is the local Green function of the homogeneous superconductor in the absence of coupling to the adatom,

$$g(E) = \int \frac{d\mathbf{p}}{(2\pi)^3} \frac{E + \xi_\mathbf{p}\tau_z + \Delta\tau_x}{E^2 - \xi_p^2 - \Delta^2} = -\pi\nu_0 \frac{E + \Delta\tau_x}{\sqrt{\Delta^2 - E^2}}. \quad \text{(C.17)}$$

The effect of the adatom is included through the self energy

$$\Sigma(E) = t^2 (E - H_d)^{-1}. \quad \text{(C.18)}$$

The poles of $G(E)$ and hence the subgap spectrum can be found from the condition

$$\det G^{-1}(E) = \det\left[g^{-1}(E) - \Sigma(E)\right] = 0. \quad \text{(C.19)}$$

This separates into separate equations for the two spin components,

$$\det\left\{\frac{(E - \Delta\tau_x)}{\sqrt{\Delta^2 - \omega^2}} - \frac{\Gamma}{\left[(\omega \pm U/2) - (\epsilon_d - \mu + \frac{U}{2})\tau_z\right]}\right\} = 0, \quad \text{(C.20)}$$

with $\Gamma = \pi\nu_0 t^2$. In the limit $U, \Gamma \gg \Delta$, one finds subgap states with energies

$$E = \pm\Delta \frac{\Gamma^2 + (\epsilon_d - \mu + U/2)^2 - (U/2)^2}{\sqrt{(\Gamma^2 + (\epsilon_d - \mu + U/2)^2 - (U/2)^2)^2 + \Gamma^2 U^2}}. \quad \text{(C.21)}$$

When written in term of $E_{d\uparrow} = \epsilon_d - \mu$ and $E_{d\downarrow} = \epsilon_d - \mu + U$, this yields Eq. (5.9).

References

[1] J. Alicea, Rep. Prog. Phys. **75**, 076501 (2012).
[2] C.W.J. Beenakker, Annu. Rev. Con. Mat. Phys. **4**, 113 (2013).
[3] S. Das Sarma, M. Freedman, C. Nayak, arXiv:1501.02813 (2015).
[4] C.W.J. Beenakker, Rev. Mod. Phys. **87**, 1037 (2015).
[5] E. Majorana, Nuovo Cimento, **5**, 171 (1937).
[6] F. Wilczek, Nature Phys. **5**, 614 (2009).
[7] A. Kitaev, Ann. Phys. **303**, 2 (2003).
[8] C. Nayak, S.H. Simon, A. Stern, M. Freedman, and S. Das Sarma, Rev. Mod. Phys. **80**, 1083 (2008).
[9] V. Mourik, K. Zuo, S.M. Frolov, S.R. Plissard, E.P.A.M. Bakkers, and L.P. Kouwenhoven, Science **336**, 1003 (2012).
[10] A. Das, Y. Ronen, Y. Most, Y. Oreg, M. Heiblum, and H. Shtrikman, Nature Phys. **8**, 887 (2012).
[11] H.O.H. Churchill, V. Fatemi, K. Grove-Rasmussen, M.T. Deng, P. Caroff, H.Q. Xu, and C.M. Marcus, Phys. Rev. B **87**, 241401(R) (2013).
[12] M.T. Deng, C.L. Yu, G.Y. Huang, M. Larsson, P. Caroff, and H.Q. Xu, Nano Lett. **12**, 6414 (2012).
[13] L.P. Rokhinson, X. Liu, and J.K. Furdyna, Nature Phys. **8**, 795 (2012).
[14] A.D.K. Finck, D.J. Van Harlingen, P.K. Mohseni, K. Jung, and X. Li, Phys. Rev. Lett. **110**, 126406 (2013).
[15] S. Nadj-Perge, I.K. Drozdov, J. Li, H. Chen, S. Jeon, J. Seo, A.H. MacDonald, B.A. Bernevig, A. Yazdani, Science **346**, 602 (2014).
[16] W. Chang, S.M. Albrecht, T.S. Jespersen, F. Kuemmeth, P. Krogstrup, J. Nygard, C.M. Marcus, Nature Nanotech. **10**, 232 (2015).
[17] M. Ruby, F. Pientka, Y. Peng, F. von Oppen, B.W. Heinrich, K.J. Franke, arXiv:1506.06763 (2015).
[18] A.Y. Kitaev, Phys. Usp. **44**, 131 (2001).
[19] R. Jackiw and C. Rebbi, Phys. Rev. D **13** 3398 (1976).
[20] S. Ryu, A.P. Schnyder, A. Furusaki, and A.W.W. Ludwig, New J. Phys., **12**, 065010 (2010).
[21] L. Fu and C.L. Kane, Phys. Rev. Lett. **100**, 096407 (2008).
[22] L. Fu and C.L. Kane, Phys. Rev. B **79**, 161408R (2009).
[23] L. Jiang, D. Pekker, J. Alicea, G. Refael, Y. Oreg, A. Brataas, and F. von Oppen, Phys. Rev. B **87**, 075438 (2013).
[24] R.M. Lutchyn, J.D. Sau, and S. Das Sarma, Phys. Rev. Lett. **105**, 077001 (2010).
[25] Y. Oreg, G. Refael, and F. von Oppen, Phys. Rev. Lett. **105**, 177002 (2010).
[26] S. Nadj-Perge, I.K. Drozdov, B.A. Bernevig, and A. Yazdani, Phys. Rev. B **88**, 020407(R) (2013).

[27] L. Yu, Acta Phys. Sin. **21**, 75 (1965).
[28] H. Shiba, Prog. Theor. Phys. **40**, 435 (1968).
[29] A.I. Rusinov, Zh. Eksp. Teor. Fiz. Pisma Red. **9**, 146 (1968) [JETP Lett. **9**, 85 (1969)].
[30] A.V. Balatsky, I. Vekhter, and J.-X. Zhu, Rev. Mod. Phys. **78**, 373 (2006).
[31] A. Yazdani, B.A. Jones, C.P. Lutz, M.F. Crommie, and D.M. Eigler, Science **275**, 1767 (1997).
[32] A. Yazdani, C.M. Howald, C.P. Lutz, A. Kapitulnik, and D.M. Eigler, Phys. Rev. Lett. **83**, 176 (1999).
[33] H. Shiba, Prog. Theor. Phys. **50**, 50 (1973).
[34] P. W. Anderson, Phys. Rev. **124**, 41 (1961).
[35] F. Pientka, L. Glazman, F. von Oppen, Phys. Rev. B **88**, 155420 (2013).
[36] F. Pientka, L.I. Glazman, F. von Oppen, Phys. Rev. B **89**, 180505(R) (2014).
[37] J. Klinovaja, P. Stano, A. Yazdani, and D. Loss, Phys. Rev. Lett. **111**, 186805 (2013).
[38] B. Braunecker and P. Simon, Phys. Rev. Lett. **111**, 147202 (2013).
[39] M.M. Vazifeh and M. Franz, Phys. Rev. Lett. **111**, 206802 (2013).
[40] J. Li, H. Chen, I.K. Drozdov, A. Yazdani, B.A. Bernevig, A.H. MacDonald, Phys. Rev. B **90**, 235433 (2014).
[41] B. Braunecker, G.I. Japaridze, J. Klinovaja, and D. Loss, Phys. Rev. B **82**, 045127 (2010).
[42] Y. Peng, F. Pientka, L.I. Glazman, and F. von Oppen, Phys. Rev. Lett. **114**, 106801 (2015).
[43] N. Read and D. Green, Phys. Rev. B **61**, 10267 (2000).
[44] D.A. Ivanov, Phys. Rev. Lett. **86**, 268 (2001).
[45] A. Stern, F. von Oppen, E. Mariani, Phys. Rev. B **70**, 205338 (2004).
[46] J. Alicea, Y. Oreg, G. Refael, and F. von Oppen, M.P.A. Fisher, Nature Phys. **7**, 412 (2011).
[47] A. Romito, J. Alicea, G. Refael, and F. von Oppen, Phys. Rev. B **85**, 020502(R) (2012).
[48] J.D. Sau, D.J. Clarke, and S. Tewari, Phys. Rev. B **84**, 094505 (2011).
[49] B. van Heck, A.R. Akhmerov, F. Hassler, M. Burrello, and C.W.J. Beenakker, New J. Phys. **14**, 035019 (2012).
[50] M.V. Berry, Proc. Roy. Soc. A **392**, 45 (1984).
[51] F. Wilczek and A. Zee, Phys. Rev. Lett. **52**, 2111 (1984).
[52] F. Pientka, G. Kells, A. Romito, P.W. Brouwer, F. von Oppen, Phys. Rev. Lett. **109**, 227006 (2012).
[53] K.T. Law, P.A. Lee, T.K. Ng, Phys. Rev. Lett. **103**, 237001 (2009).
[54] K. Flensberg, Phys. Rev. B **82**, 180516 (2010).
[55] I. Martin and D. Mozyrsky, Phys. Rev. B **90**, 100508 (2014).
[56] M. Ruby, F. Pientka, Y. Peng, F. von Oppen, B.W. Heinrich, K.J. Franke, Phys. Rev. Lett. **115**, 087001 (2015).
[57] Y. Peng, F. Pientka, Y. Vinkler-Aviv, L.I. Glazman, F. von Oppen, arXiv:1506.06763 (2015).
[58] D. Badiane, M. Houzet, J.S. Meyer, Phys. Rev. Lett. **107** 177002 (2011)